Chapter 6

Second-Order Statistics: Weak Fluctuation Theory

Overview: The main purpose of this chapter is to introduce the *mutual coherence function* (MCF), which is a two-point field moment. It is used to determine the additional *beam spreading* caused by atmospheric turbulence over that due to diffraction alone, and to determine the *spatial coherence radius* of the wave at the receiver pupil plane. Knowledge of beam spreading is important in a free space optics (FSO) communications link, for example, because it determines the *loss of power* at the receiver. Also, the spatial coherence radius defines the *effective receiver aperture size* in a heterodyne detection system.

The *mean irradiance* is obtained from the MCF when the two points in the MCF coincide. For the special case when both points are zero, the resulting expression corresponds to the maximum mean irradiance on the beam optical axis from which we deduce the *long-term beam radius.*

The normalized MCF defines the *modulus of the complex degree of coherence* (DOC) from which the *wave structure function* (WSF) is identified (and hence, the *log-amplitude* and *phase structure functions* are also identified). The separation distance at which the DOC falls to $1/e$ defines the spatial coherence radius ρ_0. The root-mean-square (rms) *angle-of-arrival* and rms *image jitter* are both derived from the phase structure function.

Movement of the short-term beam instantaneous center (or "hot spot") is commonly called *beam wander.* A new model for rms beam wander displacement is developed here by analyzing the refractive effects of turbulent eddies equal to or larger than the beam up to the outer scale of turbulence. An estimate of the *short-term beam radius* is then obtained by removing beam wander effects from the long-term beam radius.

Expressions for the beam spot size and spatial coherence radius derived here are based on *weak fluctuation theory* using the *Rytov method.* Many of the results that we develop are based on the *Kolmogorov power-law spectrum* for reasons of mathematical simplicity. However, in attempting to compare models with measured data taken in outdoor experiments, it may be necessary to use models found in Appendix III based on the *modified atmospheric spectrum* because it is a better representation of actual atmospheric conditions.

Flowchart

In Chaps. 6 and 7 we examine the first and second moment of the optical field from which we can deduce several important statistical quantities. The flowchart provided in Table 6.1 below is intended to help the reader identify how these various statistical quantities are related back to the optical field in the presence of optical turbulence.

Table 6.1 Flowchart for Chaps. 6 and 7.

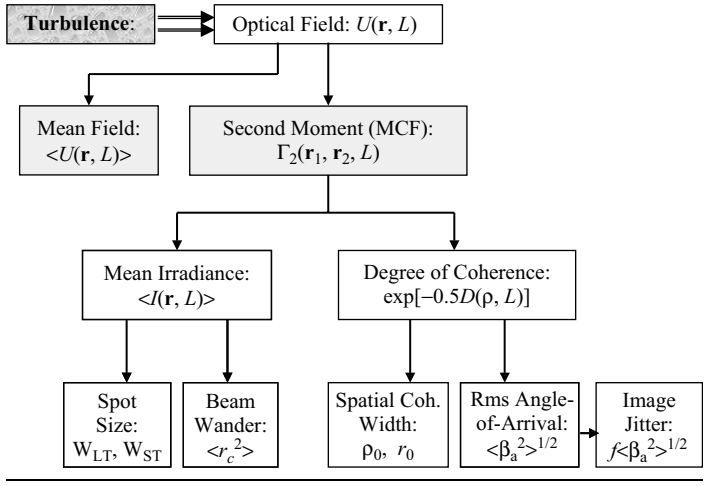

6.1 Introduction

Optical wave propagation through a random medium characterized by small fluctuations in the refractive index has been the subject of extensive theoretical investigations for many years [1–11]. Random fluctuations in the index of refraction cause spreading of the beam beyond that due to pure diffraction, random wandering of the instantaneous beam center (beam wander), loss of spatial coherence, and random fluctuations in the irradiance and phase. Scale sizes larger than the beam diameter cause beam wander, whereas scale sizes on the order of the first Fresnel zone are the primary cause of irradiance fluctuations (scintillations). Knowledge of the behavior of an optical wave in turbulence is important in optical communications, laser radar, imaging, adaptive optics, target designation, ranging, and remote sensing, among other areas.

Historically, many of the classical treatments [1,2] of optical wave propagation were concerned with uniform plane waves and spherical waves. These simple optical wave models are useful in describing certain aspects of wave propagation in turbulence but, because of their inherent infinite extent, are not adequate in describing laser beams when focusing effects and finite size of the transmitted wave must be taken into account. In addition, classical studies of wave propagation based on the Rytov method made use of only the first-order approximation. As a consequence, these particular studies were generally limited to calculations of the log-amplitude variance, phase variance, covariance functions, or various structure functions, all of which can be described by the first-order perturbation. General field moments of the optical wave, including the mean field and mean irradiance, require both first- *and* second-order Rytov approximations [12,13].

In this chapter and in Chap. 7 we develop tractable expressions for various specializations of the second-order field moment associated with *line-of-sight propagation.* Here we derive our results using *weak-fluctuation theory* as

developed in Chap. 5 (Section 5.2.2), whereas in Chap. 7 we derive some of these results once again for the *strong fluctuation regime.* Most analytic expressions obtained in these chapters are based on a *constant* refractive-index structure parameter C_n^2, characteristic of a near-ground *horizontal propagation path.* However, when considering slant paths or vertical paths, we do account for variations in C_n^2 along the path. Problems of this latter type are further discussed in Chap.12 in regard to laser satellite communication systems.

6.2 Basic Concepts

In most applications we characterize the received wave in terms of statistical moments of the random optical field $U(\mathbf{r}, L)$, where L is the propagation distance along the positive z-axis from the emitting aperture of the transmitter to the receiver and $\mathbf{r}$ is a vector in the receiver plane transverse to the propagation axis. The *first moment* $\langle U(\mathbf{r}, L)\rangle$, where the brackets $\langle\ \rangle$ denote an ensemble average, describes the *coherent portion* of the field. The *mutual coherence function* (MCF) of the wave is defined by the *second moment*

$$\Gamma_2(\mathbf{r}_1, \mathbf{r}_2, L) = \langle U(\mathbf{r}_1, L)U^*(\mathbf{r}_2, L)\rangle, \tag{1}$$

where $\mathbf{r}_1$ and $\mathbf{r}_2$ are observation points in the receiver plane and $U^*(\mathbf{r}, L)$ denotes the complex conjugate field. For identical observation points, the MCF determines the *mean irradiance* from which turbulence-induced beam spread is deduced. Also obtained from the MCF is the *modulus of the complex degree of coherence* that describes the loss of spatial coherence of an initially coherent wave. Among other applications, this latter quantity is important in determining the signal-to-noise ratio (SNR) of an optical heterodyne detector and the limiting resolution obtainable for an imaging system. Fluctuations in the irradiance of the field are described by the *cross-coherence function* of the field or *fourth-order moment*

$$\Gamma_4(\mathbf{r}_1, \mathbf{r}_2, \mathbf{r}_3, \mathbf{r}_4, L) = \langle U(\mathbf{r}_1, L)U^*(\mathbf{r}_2, L)U(\mathbf{r}_3, L)U^*(\mathbf{r}_4, L)\rangle. \tag{2}$$

Specializations of the fourth moment lead to the *second moment of irradiance* that, along with the mean irradiance, is used to define the *scintillation index* (see Chaps. 8 and 9). The fourth moment is also necessary to calculate the *irradiance covariance function*, from which the *irradiance correlation width* is deduced.

6.2.1 Free-space analysis

The free-space analysis of a lowest-order Gaussian-beam wave was given in Chap. 4. To review, we assume the transmitted wave is a *unit-amplitude* Gaussian beam that, in the plane of the emitting aperture of the transmitter at $z = 0$, can be expressed as

$$z = 0: \quad U_0(\mathbf{r}, 0) = \exp\left(-\frac{r^2}{W_0^2} - i\frac{kr^2}{2F_0}\right), \tag{3}$$

where F_0 and W_0 denote the phase front radius of curvature and beam radius, respectively, and k is the optical wave number. The free-space optical wave in the receiver plane at $z = L$ is another Gaussian beam described by

$$z = L: \quad U_0(\mathbf{r}, L) = \frac{1}{p(L)} \exp(ikL) \exp\left(-\frac{r^2}{W^2} - i\frac{kr^2}{2F}\right), \tag{4}$$

where F and W denote the receiver plane phase front radius of curvature and beam radius, respectively, and

$$p(L) = 1 - \frac{L}{F_0} + i\frac{2L}{kW_0^2}. \tag{5}$$

Following the approach used in Section 4.4.1, the real and imaginary parts of the propagation parameter $p(L) = \Theta_0 + i\Lambda_0$ are used to introduce the nondimensional *input plane beam parameters*

$$\Theta_0 = 1 - \frac{L}{F_0}, \qquad \Lambda_0 = \frac{2L}{kW_0^2}. \tag{6}$$

Similarly, the reciprocal quantity $1/p(L) = \Theta - i\Lambda$ leads to the nondimensional *output plane beam parameters*

$$\begin{aligned} \Theta &= 1 + \frac{L}{F} = \frac{\Theta_0}{\Theta_0^2 + \Lambda_0^2}, \\ \overline{\Theta} &= -\frac{L}{F} = 1 - \Theta, \\ \Lambda &= \frac{2L}{kW^2} = \frac{\Lambda_0}{\Theta_0^2 + \Lambda_0^2}. \end{aligned} \tag{7}$$

Either set of beam parameters can be used to characterize the Gaussian-beam wave, but in the following analysis we find that mathematical expressions for the output plane statistics are more conveniently represented in terms of the output plane parameters (7).

6.2.2 Rytov method

In the absence of optical elements between input (transmitter) and output (receiver) planes, the propagation channel is characterized as *line-of-sight* propagation, i.e., the receiver can "see" the transmitter. Such propagation problems under weak fluctuations can be analyzed by the *classical Rytov method* [1,7], which assumes the optical field at propagation distance L from the transmitter is represented by (see Chap. 5)

$$\begin{aligned} U(\mathbf{r}, L) &= U_0(\mathbf{r}, L) \exp[\psi(\mathbf{r}, L)] \\ &= U_0(\mathbf{r}, L) \exp\big[\psi_1(\mathbf{r}, L) + \psi_2(\mathbf{r}, L) + \cdots\big], \end{aligned} \tag{8}$$

where $U_0(\mathbf{r}, L)$ is the free-space Gaussian-beam wave at the receiver. Here, $\psi(\mathbf{r}, L)$ is the total *complex phase perturbation* of the field due to random inhomogeneities

along the propagation path, and $\psi_1(\mathbf{r}, L)$ and $\psi_2(\mathbf{r}, L)$ are *first-* and *second-order* perturbations, respectively.

The *long-time-average* statistical moments of the optical field (8) of greatest interest in optical wave propagation involve the following ensemble averages of the first- and second-order complex phase perturbations:

$$\big\langle \exp[\psi(\mathbf{r}, L)] \big\rangle = \big\langle \exp\big[\psi_1(\mathbf{r}, L) + \psi_2(\mathbf{r}, L)\big] \big\rangle, \tag{9}$$

$$\big\langle \exp[\psi(\mathbf{r}_1, L) + \psi^*(\mathbf{r}_2, L)] \big\rangle = \big\langle \exp\big[\psi_1(\mathbf{r}_1, L) + \psi_2(\mathbf{r}_1, L) + \psi_1^*(\mathbf{r}_2, L) + \psi_2^*(\mathbf{r}_2, L)\big] \big\rangle, \tag{10}$$

$$\begin{aligned} &\big\langle \exp\big[\psi_1(\mathbf{r}_1, L) + \psi^*(\mathbf{r}_2, L) + \psi(\mathbf{r}_3, L) + \psi^*(\mathbf{r}_4, L)\big] \big\rangle, \\ &\quad = \big\langle \exp\big[\psi_1(\mathbf{r}_1, L) + \psi_2(\mathbf{r}_1, L) + \psi_1^*(\mathbf{r}_2, L) + \psi_2^*(\mathbf{r}_2, L) \\ &\qquad + \psi_1(\mathbf{r}_3, L) + \psi_2(\mathbf{r}_3, L) + \psi_1^*(\mathbf{r}_4, L) + \psi_2^*(\mathbf{r}_4, L)\big] \big\rangle. \end{aligned} \tag{11}$$

In calculating the above moments, we use the method of cumulants [14] defined by

$$\begin{aligned} \langle \exp(\psi) \rangle &= \lim_{t \to -i} \langle \exp(it\psi) \rangle \\ &= \exp\left(K_1 + \frac{1}{2} K_2 + \frac{1}{6} K_3 + \frac{1}{24} K_4 + \cdots \right), \end{aligned} \tag{12}$$

where

$$\begin{aligned} K_1 &= \langle \psi \rangle, \\ K_2 &= \langle \psi^2 \rangle - \langle \psi \rangle^2, \\ K_3 &= \langle \psi^3 \rangle - 3\langle \psi \rangle \langle \psi^2 \rangle + 2\langle \psi \rangle^3, \\ K_4 &= \langle \psi^4 \rangle - 4\langle \psi \rangle \langle \psi^3 \rangle - 3\langle \psi^2 \rangle^2 + 12\langle \psi^2 \rangle \langle \psi \rangle^2 - 6\langle \psi \rangle^4, \end{aligned} \tag{13}$$

and so on. Theoretically, we can use the method of cumulants to calculate moments of all orders in the Rytov approximation. However, spectral representations are normally developed only for first-order and second-order approximations. Including terms up to those of second order in the Rytov approximation, Eq. (12) reduces to

$$\begin{aligned} \langle \exp(\psi) \rangle &= \exp\left(K_1 + \frac{1}{2} K_2 \right) \\ &= \exp\left[\langle \psi \rangle + \frac{1}{2} \big(\langle \psi^2 \rangle - \langle \psi \rangle^2 \big) \right], \end{aligned} \tag{14}$$

which is an exact relation only in the case where ψ is a Gaussian random variable.

The use of (14) to evaluate the first-, second-, and fourth-order moments (9–11) leads to the following relations (see Prob. 4):

$$\langle \exp[\psi(\mathbf{r}, L)] \rangle = \exp[E_1(0,0)], \tag{15}$$

$$\langle \exp[\psi(\mathbf{r}_1, L) + \psi^*(\mathbf{r}_2, L)] \rangle = \exp[2E_1(0,0) + E_2(\mathbf{r}_1, \mathbf{r}_2)], \tag{16}$$

$$\begin{aligned} &\langle \exp[\psi(\mathbf{r}_1, L) + \psi^*(\mathbf{r}_2, L) + \psi(\mathbf{r}_3, L) + \psi^*(\mathbf{r}_4, L)] \rangle \\ &\quad = \exp[4E_1(0,0) + E_2(\mathbf{r}_1, \mathbf{r}_2) + E_2(\mathbf{r}_1, \mathbf{r}_4) \\ &\qquad + E_2(\mathbf{r}_3, \mathbf{r}_2) + E_2(\mathbf{r}_3, \mathbf{r}_4) + E_3(\mathbf{r}_1, \mathbf{r}_3) + E_3^*(\mathbf{r}_2, \mathbf{r}_4)], \end{aligned} \tag{17}$$

where $E_1(0,0)$, $E_2(\mathbf{r}_1, \mathbf{r}_2)$, and $E_3(\mathbf{r}_1, \mathbf{r}_2)$ are integrals defined by Eqs. (65)–(67) in Chap. 5. Based on these results, it follows that *all* statistical quantities of interest can be expressed as certain linear combinations of the integrals

$$\begin{aligned} E_1(0,0) &= \langle \psi_2(\mathbf{r}, L) \rangle + \frac{1}{2} \langle \psi_1^2(\mathbf{r}, L) \rangle \\ &= -2\pi^2 k^2 \int_0^L \int_0^\infty \kappa \Phi_n(\kappa, z)\, d\kappa\, dz, \end{aligned} \tag{18}$$

$$\begin{aligned} E_2(\mathbf{r}_1, \mathbf{r}_2) &= \langle \psi_1(\mathbf{r}_1, L) \psi_1^*(\mathbf{r}_2, L) \rangle \\ &= 4\pi^2 k^2 \int_0^L dz \int_0^\infty d\kappa \kappa \Phi_n(\kappa, z) J_0(\kappa |\gamma \mathbf{r}_1 - \gamma^* \mathbf{r}_2|) \\ &\quad \times \exp\left[-\frac{i\kappa^2}{2k} (\gamma - \gamma^*)(L - z) \right] \\ &= 4\pi^2 k^2 \int_0^L \int_0^\infty \kappa \Phi_n(\kappa, z) J_0 \left\{ \kappa \left| \left[1 - \overline{\Theta}(1 - z/L) \right] \mathbf{p} \right. \right. \\ &\quad \left. \left. - 2i\Lambda(1 - z/L)\mathbf{r} \right| \right\} \exp\left[-\frac{\Lambda L \kappa^2 (1 - z/L)^2}{k} \right] d\kappa\, dz, \end{aligned} \tag{19}$$

$$\begin{aligned} E_3(\mathbf{r}_1, \mathbf{r}_2) &= \langle \psi_1(\mathbf{r}_1, L) \psi_1(\mathbf{r}_2, L) \rangle \\ &= -4\pi^2 k^2 \int_0^L dz \int_0^\infty d\kappa \kappa \Phi_n(\kappa, z) \\ &\quad \times J_0(\gamma \kappa |\mathbf{r}_1 - \mathbf{r}_2|) \exp\left[-\frac{i\kappa^2 \gamma}{k} (L - z) \right] \\ &= -4\pi^2 k^2 \int_0^L \int_0^\infty \kappa \Phi_n(\kappa, z) J_0 \left\{ \kappa \rho \left[1 - (\overline{\Theta} + i\Lambda)(1 - z/L) \right] \right\} \\ &\quad \times \exp\left[-\frac{\Lambda L \kappa^2 (1 - z/L)^2}{k} \right] \\ &\quad \times \exp\left\{ -\frac{iL\kappa^2}{k} (1 - z/L) \left[1 - \overline{\Theta}(1 - z/L) \right] \right\} d\kappa\, dz, \end{aligned} \tag{20}$$

where we have introduced the center of gravity and difference vectors

$$\begin{aligned} \mathbf{r} &= \frac{1}{2}(\mathbf{r}_1 + \mathbf{r}_2), \qquad \mathbf{p} = \mathbf{r}_1 - \mathbf{r}_2, \\ r &= |\mathbf{r}|, \ \rho = |\mathbf{p}| \end{aligned} \tag{21}$$

and expressed the path amplitude ratio γ in terms of the Gaussian-beam parameters Θ and Λ according to

$$\gamma = \frac{p(z)}{p(L)} = 1 - (\overline{\Theta} + i\Lambda)(1 - z/L), \qquad 0 \le z \le L. \tag{22}$$

Clearly, $\gamma = 1$ in the limiting case of a *plane wave* ($\Theta = 1$, $\Lambda = 0$), whereas $\gamma = z/L$ for a *spherical wave* ($\Theta = \Lambda = 0$).

Note: The absolute value bars inside the argument of the Bessel function in Eq. (19) refer only to the vectors, not the complex quantities involving $i = \sqrt{-1}$.

For horizontal propagation paths it is customary to treat the refractive-index structure parameter C_n^2 as constant so that we can set $\Phi_n(\kappa, z) = \Phi_n(\kappa)$. To further simplify the above expressions (18)–(20), it is useful to introduce the normalized distance variable $\xi = 1 - z/L$. By doing so, the path amplitude ratio (22) becomes

$$\gamma = 1 - (\overline{\Theta} + i\Lambda)\xi, \qquad 0 \le \xi \le 1. \tag{23}$$

Consequently, Eqs. (18)–(20) can be expressed in the form

$$E_1(0,0) = -2\pi^2 k^2 L \int_0^\infty \kappa \Phi_n(\kappa)\, d\kappa, \tag{24}$$

$$\begin{aligned} E_2(\mathbf{r}_1, \mathbf{r}_2) = 4\pi^2 k^2 L \int_0^1 \int_0^\infty \kappa \Phi_n(\kappa) \\ \times J_0\big[\kappa\big|(1 - \overline{\Theta}\xi)\mathbf{p} - 2i\Lambda\xi\mathbf{r}\big|\big] \exp\left(-\frac{\Lambda L \kappa^2 \xi^2}{k}\right) d\kappa\, d\xi, \end{aligned} \tag{25}$$

$$\begin{aligned} E_3(\mathbf{r}_1, \mathbf{r}_2) = -4\pi^2 k^2 L \int_0^1 \int_0^\infty \kappa \Phi_n(\kappa) J_0\big[(1 - \overline{\Theta}\xi - i\Lambda\xi)\kappa\rho\big] \\ \times \exp\left(-\frac{\Lambda L \kappa^2 \xi^2}{k}\right) \exp\left[-\frac{iL\kappa^2}{k}\xi\big(1 - \overline{\Theta}\xi\big)\right] d\kappa\, d\xi. \end{aligned} \tag{26}$$

6.2.3 Mean value of the field

The coherent portion of the optical field is described by the *mean field*

$$\begin{aligned} \langle U(\mathbf{r}, L)\rangle &= U_0(\mathbf{r}, L)\langle \exp[\psi(\mathbf{r}, L)]\rangle \\ &= U_0(\mathbf{r}, L) \exp[E_1(0,0)], \end{aligned} \tag{27}$$

where $E_1(0, 0)$ is defined by Eq. (24). The integral in (24) does not converge for a simple power-law Kolmogorov spectrum extended to all wave numbers because of the singularity at $\kappa = 0$. However, for the von Kármán spectrum [Eq. (20) in Chap. 3]

$$\Phi_n(\kappa) = 0.033 C_n^2 \frac{\exp\left(-\kappa^2/\kappa_m^2\right)}{(\kappa^2 + \kappa_0^2)^{11/6}}, \tag{28}$$

it leads to[1] (see Prob. 2)

$$\begin{aligned} E_1(0,0) &= -0.033\pi^2 C_n^2 k^2 L \kappa_0^{-5/3} U(1; 1/6; \kappa_0^2/\kappa_m^2) \\ &\cong -0.39 C_n^2 k^2 L \kappa_0^{-5/3}, \quad \kappa_0^2/\kappa_m^2 \ll 1, \end{aligned} \tag{29}$$

where $\kappa_0 \sim 1/L_0$, $\kappa_m = 5.92/l_0$, and L_0 and l_0 are outer scale and inner scale, respectively. The condition $\kappa_0^2/\kappa_m^2 \ll 1$, roughly the same as $(l_0/L_0)^2 \ll 1$, is always satisfied in the atmosphere. The function $U(a; c; x)$ is the confluent hypergeometric function of the second kind [15] (also, see Appendix I), which we have replaced in the last step of (29) by use of the asymptotic formula

$$U(a; c; x) \sim \frac{\Gamma(1-c)}{\Gamma(1+a-c)}, \qquad 0 < c < 1, \quad x \to 0^+. \tag{30}$$

Combining the above results, we find that the *mean field* is given by

$$\langle U(\mathbf{r}, L)\rangle = U_0(\mathbf{r}, L) \exp\left(-0.39 C_n^2 k^2 L \kappa_0^{-5/3}\right). \tag{31}$$

Consequently, for visible and IR wavelengths, the mean field (31) tends to zero in the first few meters of the propagation path.

6.3 Mutual Coherence Function

The *second-order moment*, or MCF, is defined by the ensemble average

$$\Gamma_2(\mathbf{r}_1, \mathbf{r}_2, L) = \langle U(\mathbf{r}_1, L) U^*(\mathbf{r}_2, L)\rangle, \tag{32}$$

which, under weak fluctuation theory, becomes [16,17]

$$\begin{aligned} \Gamma_2(\mathbf{r}_1, \mathbf{r}_2, L) &= U_0(\mathbf{r}_1, L) U_0^*(\mathbf{r}_2, L) \left\langle \exp[\psi(\mathbf{r}_1, L) + \psi^*(\mathbf{r}_2, L)] \right\rangle \\ &= \Gamma_2^0(\mathbf{r}_1, \mathbf{r}_2, L) \exp[2E_1(0,0) + E_2(\mathbf{r}_1, \mathbf{r}_2)]. \end{aligned} \tag{33}$$

In arriving at the second step in (33), we have used Eq. (16) and recognized the first factor on the right-hand side as the free-space MCF defined by

$$\begin{aligned} \Gamma_2^0(\mathbf{r}_1, \mathbf{r}_2, L) &= U_0(\mathbf{r}_1, L) U_0^*(\mathbf{r}_2, L) \\ &= \frac{W_0^2}{W^2} \exp\left(-\frac{2r^2}{W^2} - \frac{\rho^2}{2W^2} - i\frac{k}{F}\mathbf{p}\cdot\mathbf{r}\right). \end{aligned} \tag{34}$$

[1] In Section 8.6.1 we identify $E_1(0, 0) \cong -0.5\sigma_S^2(L)$, where $\sigma_S^2(L)$ is the phase variance.

Upon replacing $E_1(0,0)$ and $E_2(\mathbf{r}_1, \mathbf{r}_2)$ by integrals (24) and (25), the MCF (33) takes the specific form

$$\Gamma_2(\mathbf{r}_1, \mathbf{r}_2, L) = \Gamma_2^0(\mathbf{r}_1, \mathbf{r}_2, L) \exp\left[\!\!\left[-4\pi^2 k^2 L \int_0^1 \int_0^\infty \kappa \Phi_n(\kappa) \right.\right.$$
$$\left.\left. \times \left\{ 1 - \exp\left(-\frac{\Lambda L \kappa^2 \xi^2}{k} \right) J_0\left[\left| \left(1 - \overline{\Theta}\xi\right)\mathbf{p} - 2i\Lambda\xi\mathbf{r} \right| \kappa \right] \right\} d\kappa d\xi \right]\!\!\right]. \tag{35}$$

Rather than evaluate (35) directly, it is helpful for interpretation purposes to group terms according to

$$\Gamma_2(\mathbf{r}_1, \mathbf{r}_2, L) = \Gamma_2^0(\mathbf{r}_1, \mathbf{r}_2, L) \exp\left[\sigma_r^2(\mathbf{r}_1, L) + \sigma_r^2(\mathbf{r}_2, L) - T\right] \exp\left[-\frac{1}{2}\Delta(\mathbf{r}_1, \mathbf{r}_2, L) \right], \tag{36}$$

where

$$\sigma_r^2(\mathbf{r}, L) = \frac{1}{2}[E_2(\mathbf{r}, \mathbf{r}) - E_2(0,0)]$$
$$= 2\pi^2 k^2 L \int_0^1 \int_0^\infty \kappa \Phi_n(\kappa) \exp\left(-\frac{\Lambda L \kappa^2 \xi^2}{k} \right)$$
$$\times [I_0(2\Lambda r \xi \kappa) - 1]\, d\kappa\, d\xi, \tag{37}$$

$$T = -2E_1(0,0) - E_2(0,0)$$
$$= 4\pi^2 k^2 L \int_0^1 \int_0^\infty \kappa \Phi_n(\kappa) \left[1 - \exp\left(-\frac{\Lambda L \kappa^2 \xi^2}{k} \right) \right] d\kappa\, d\xi, \tag{38}$$

$$\Delta(\mathbf{r}_1, \mathbf{r}_2, L) = E_2(\mathbf{r}_1, \mathbf{r}_1) + E_2(\mathbf{r}_2, \mathbf{r}_2) - 2E_2(\mathbf{r}_1, \mathbf{r}_2)$$
$$= 4\pi^2 k^2 L \int_0^1 \int_0^\infty \kappa \Phi_n(\kappa) \exp\left(-\frac{\Lambda L \kappa^2 \xi^2}{k} \right) \tag{39}$$
$$\times \left\{ I_0(2\Lambda r_1 \xi \kappa) + I_0(2\Lambda r_2 \xi \kappa) - 2J_0\left[\left| \left(1 - \overline{\Theta}\xi\right)\mathbf{p} - 2i\Lambda\xi\mathbf{r} \right| \kappa \right] \right\} d\kappa\, d\xi,$$

and $I_0(x) = J_0(ix)$ is the modified Bessel function (see Appendix I). Physically, the quantity $\sigma_r^2(\mathbf{r}, L)$ describes the atmospherically induced change in the mean irradiance profile in the transverse direction, whereas the quantity T, which is independent of $\mathbf{r}$, describes the change in the on-axis mean irradiance at the receiver plane caused by turbulence. The last exponential function in (36) is the complex degree of coherence for which $\mathrm{Re}[\Delta(\mathbf{r}_1, \mathbf{r}_2, L)] = D(\mathbf{r}_1, \mathbf{r}_2, L)$ is the *wave structure function* (WSF) of the Gaussian-beam wave.

6.3.1 Mean irradiance and turbulence-induced beam spreading

The MCF (36) evaluated at identical observation points $\mathbf{r}_1 = \mathbf{r}_2 = \mathbf{r}$ leads to the *mean irradiance*

$$\begin{aligned}\langle I(\mathbf{r}, L)\rangle &= \Gamma_2(\mathbf{r}, \mathbf{r}, L) \\ &= \frac{W_0^2}{W^2}\exp\left(-\frac{2r^2}{W^2}\right)\exp\left[2\sigma_r^2(\mathbf{r}, L) - T\right],\end{aligned} \tag{40}$$

from which the additional beam spread due to turbulence can be deduced. Under the assumption of the Kolmogorov power-law spectrum [Eq. (18) in Chap. 3]

$$\Phi_n(\kappa) = 0.033 C_n^2 \kappa^{-11/3}, \tag{41}$$

the evaluation of $\sigma_r^2(\mathbf{r}, L)$ defined by (37) yields [18] (see Prob. 9)

$$\begin{aligned}\sigma_r^2(\mathbf{r}, L) &= 0.66\sigma_R^2\Lambda^{5/6}\left[1 - {}_1F_1\left(-\frac{5}{6}; 1; \frac{2r^2}{W^2}\right)\right] \\ &\cong 1.11\sigma_R^2\Lambda^{5/6}\frac{r^2}{W^2}, \qquad r < W,\end{aligned} \tag{42}$$

where $\sigma_R^2 = 1.23 C_n^2 k^{7/6} L^{11/6}$ is the *Rytov variance* and the confluent hypergeometric function ${}_1F_1(a; c; x)$ has been replaced by its small argument approximation in the last step (see Appendix I), causing the restriction $r < W$. Again using the Kolmogorov spectrum (41), the quantity T defined by (38) similarly leads to (see Prob. 10)

$$T = 1.33\sigma_R^2\Lambda^{5/6}. \tag{43}$$

By writing $\sigma_r^2(\mathbf{r}, L) = 0.83 T r^2/W^2 \cong T r^2/W^2$ and employing the approximations

$$e^{-T} \cong \frac{1}{1+T}, \quad \frac{r^2}{W^2} - \sigma_r^2(\mathbf{r}, L) \cong \frac{r^2}{W^2(1+T)}, \tag{44}$$

we deduce that the mean irradiance profile (40) can be approximated by the Gaussian function (see Example 3 in the Worked Examples)

$$\langle I(\mathbf{r}, L)\rangle \cong \frac{W_0^2}{W_{\mathrm{LT}}^2}\exp\left(-\frac{2r^2}{W_{\mathrm{LT}}^2}\right), \qquad [\mathrm{W/m^2}] \tag{45}$$

where W_{LT} is a measure of the *effective* or *long-term beam spot size* given by

$$\begin{aligned}W_{\mathrm{LT}} &= W\sqrt{1+T} \\ &= W\sqrt{1 + 1.33\sigma_R^2\Lambda^{5/6}}.\end{aligned} \tag{46}$$

Thus, as in free space, the turbulence-induced mean irradiance (45) is completely determined by beam spot size.

Inner scale and outer scale effects on the long-term beam spot size have also been investigated using various spectrum models [17,19]. For example, using the von Kármán spectrum (28), the implied effective beam radius is

$$\begin{aligned} W_{\mathrm{LT}} &= W\left\{1 + 4.35C_n^2 k^2 L\kappa_m^{-5/3}\left[{}_2F_1\left(-\frac{5}{6}, \frac{1}{2}; \frac{3}{2}; -\Lambda Q_m\right) - 1\right]\right. \\ &\quad \left. - 0.78C_n^2 k^2 L\kappa_0^{-5/3}\left[{}_2F_2\left(\frac{1}{2}, 1; \frac{3}{2}, \frac{1}{6}; \Lambda Q_0\right) - 1\right]\right\}^{1/2} \\ &\cong W\left\{1 + 3.54\sigma_R^2\Lambda^{5/6}\left[\frac{(1 + 0.31\Lambda Q_m)^{5/6} - 1}{(\Lambda Q_m)^{5/6}} - 0.36(\Lambda Q_0)^{1/6}\right]\right\}^{1/2}, \end{aligned} \tag{47}$$

where $Q_m = L\kappa_m^2/k$ and $Q_0 = L\kappa_0^2/k$. The hypergeometric-type functions ${}_2F_1(a,\ b;\ c;\ x)$ and ${}_2F_2(a,\ b;\ c,\ d;\ x)$ have been approximated in the last step in (47) (also, see Appendix I). Depending on the spectrum model, inner scale effects may increase or decrease the spot size, whereas the outer scale always tends to limit its size. Under weak fluctuation conditions, however, the inner scale and outer scale effects on the beam spot size are often quite small, i.e., both (46) and (47) predict similar results. For that reason, it is common in many propagation problems to use the simpler model (46) to describe the turbulence-induced beam spot size.

6.3.2 MCF for plane wave and spherical wave

In the special case of a plane wave ($\Theta = 1$, $\Lambda = 0$), the MCF (35) reduces to

$$\Gamma_2(\rho, L) = \exp\left\{-4\pi^2 k^2 L\int_0^\infty \kappa\Phi_n(\kappa)[1 - J_0(\kappa\rho)]d\kappa\right\}. \tag{48}$$

Thus, the MCF (48) is independent of the location of the two points $\mathbf{r}_1$ and $\mathbf{r}_2$ (a consequence of an infinite wave model with no phase front curvature). Under the assumption of a Kolmogorov spectrum (41), it has been shown that (48) reduces to

$$\begin{aligned} \Gamma_2(\rho, L) &= \exp\left[-\left(\frac{qk\rho^2}{L}\right)^{5/6}\right] \\ &= \exp\left(-1.46C_n^2 k^2 L\rho^{5/3}\right), \qquad l_0 \ll \rho \ll L_0, \end{aligned} \tag{49}$$

where $q = 1.22(\sigma_R^2)^{6/5}$ is sometimes used as a measure of irradiance fluctuations (or strength of turbulence) in place of the Rytov variance σ_R^2.

For the case of a spherical wave ($\Theta = \Lambda = 0$), the corresponding expression for the MCF is

$$\Gamma_2(\mathbf{p}, \mathbf{r}, L) = \frac{1}{(4\pi L)^2} \exp\left\{\frac{ik}{L}\mathbf{p}\cdot\mathbf{r} - 4\pi^2 k^2 L \int_0^1 \int_0^\infty \kappa\Phi_n(\kappa)[1 - J_0(\kappa\xi\rho)]\, d\kappa\, d\xi\right\}. \tag{50}$$

Again using the Kolmogorov spectrum, we find that (50) reduces to

$$\begin{aligned}\Gamma_2(\mathbf{p},\ \mathbf{r}, L) &= \frac{1}{(4\pi L)^2} \exp\left[\frac{ik}{L}\mathbf{p}\cdot\mathbf{r} - \frac{3}{8}\left(\frac{qk\rho^2}{L}\right)^{5/6}\right] \\ &= \frac{1}{(4\pi L)^2} \exp\left(\frac{ik}{L}\mathbf{p}\cdot\mathbf{r} - 0.55C_n^2 k^2 L\rho^{5/3}\right), \qquad l_0 \ll \rho \ll L_0.\end{aligned} \tag{51}$$

Note that, unlike a plane wave, the MCF for a spherical wave (51) involves an unimportant phase factor that depends on location of the two points within the profile at the receiver plane—a consequence of the phase front curvature of a spherical wave.

6.3.3 MCF for a Gaussian-beam wave

Because it depends on the position of the two observation points, the MCF for a Gaussian-beam wave is *statistically inhomogeneous.* However, it is a function of only the scalar distance ρ for an unbounded plane wave or when $\mathbf{r}_2 = -\mathbf{r}_1$, i.e., when the observation points are symmetrically located with respect to the beam center line (optical axis). For the latter case, the MCF (35) reduces to

$$\mathbf{r}_2 = -\mathbf{r}_1\colon \quad \Gamma_2(\rho, L) = \frac{W_0^2}{W^2} \exp\left[-T - \frac{1}{4}\Lambda\left(\frac{k\rho^2}{L}\right) - \frac{1}{2}d(\rho, L)\right], \tag{52}$$

where

$$d(\rho, L) = 8\pi^2 k^2 L \int_0^1 \int_0^\infty \kappa\Phi_n(\kappa) \exp\left(-\frac{\Lambda L\kappa^2\xi^2}{k}\right)\left\{1 - J_0\left[(1 - \overline{\Theta}\xi)\kappa\rho\right]\right\} d\kappa\, d\xi. \tag{53}$$

Equation (52), normalized by its on-axis value $\Gamma_2(0, L) = (W_0^2/W^2)\exp(-T)$, can be closely approximated by [17]

$$\frac{\Gamma_2(\rho, L)}{\Gamma_2(0, L)} = \exp\left[-\frac{\Lambda}{4}\left(\frac{k\rho^2}{L}\right) - \frac{3a}{8}\left(\frac{qk\rho^2}{L}\right)^{5/6}\right], \qquad l_0 \ll \rho \ll L_0, \tag{54}$$

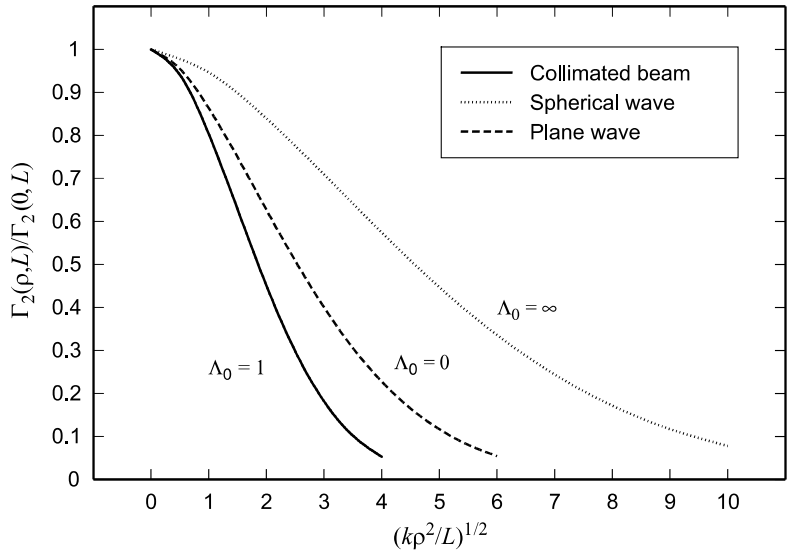

Figure 6.1 MCF (54) as predicted by the Kolmogorov spectrum, scaled by its on-axis value and shown as a function of the ratio $(k\rho^2/L)^{1/2}$ with $q = 1.22(\sigma_R^2)^{6/5} = 0.1$.

where we have used the Kolmogorov spectrum (41) and introduced

$$a = \begin{cases} \dfrac{1 - \Theta^{8/3}}{1 - \Theta}, & \Theta \geq 0 \\ \dfrac{1 + |\Theta|^{8/3}}{1 - \Theta}, & \Theta < 0. \end{cases} \tag{55}$$

The analytic approximation (54) is sufficiently accurate for most cases of interest (see Example 4 in the Worked Examples), with the possible exception of a large-aperture focused beam. In Fig. 6.1, the normalized MCF for a collimated beam (with $\Lambda_0 = 1$) is shown as a function of $(k\rho^2/L)^{1/2}$ and $q = 0.1$. For comparison purposes, the limiting cases of a plane wave ($\Lambda_0 = \Lambda = 0, a = 8/3$) and a spherical wave ($\Lambda_0 = \infty, \Lambda = 0, a = 1$) are also shown. In the spherical wave case, the phase factor that appears in (51) is eliminated because of the choice of points $\mathbf{r}_2 = -\mathbf{r}_1$ used to derive (54). Note that the MCF is widest for the spherical wave. Depending on Λ_0, the MCF for the beam wave can vary from that shown ($\Lambda_0 = 1$) in Fig. 6.1; viz., for $\Lambda_0 \ll 1$ (near field) it lies close to the plane wave limit and for $\Lambda_0 \gg 1$ (far field) it approaches the MCF for the spherical wave limit.

6.4 Spatial Coherence Radius

In addition to predicting atmospherically induced beam spreading through the mean irradiance, the MCF can also be used to predict the spatial coherence radius at the receiver plane. That is, the loss of spatial coherence of an initially

coherent beam can be deduced from the *modulus of the complex degree of coherence* (DOC)

$$\begin{aligned} \mathrm{DOC}(\mathbf{r}_1, \mathbf{r}_2, L) &= \frac{|\Gamma_2(\mathbf{r}_1, \mathbf{r}_2, L)|}{\sqrt{\Gamma_2(\mathbf{r}_1, \mathbf{r}_1, L)\Gamma_2(\mathbf{r}_2, \mathbf{r}_2, L)}} \\ &= \exp\left[-\frac{1}{2}D(\mathbf{r}_1, \mathbf{r}_2, L)\right], \end{aligned} \tag{56}$$

where $D(\mathbf{r}_1, \mathbf{r}_2, L) = \mathrm{Re}[\Delta(\mathbf{r}_1, \mathbf{r}_2, L)]$ is the *wave structure function* (WSF). Written as a function of separation distance ρ, the *spatial coherence radius* ρ_0 is defined by the $1/e$ point of the DOC (see Fig. 6.2), i.e., $D(\rho_0, L) = 2$.

The WSF is actually a sum of structure functions (see Probs. 22–24 and Section 8.6.2)

$$D(\mathbf{r}_1, \mathbf{r}_2, L) = D_\chi(\mathbf{r}_1, \mathbf{r}_2, L) + D_S(\mathbf{r}_1, \mathbf{r}_2, L), \tag{57}$$

where $D_\chi(\mathbf{r}_1, r_2, L)$ is the *log-amplitude structure function* and $D_S(\mathbf{r}_1, \mathbf{r}_2, L)$ is the *phase structure function*, the latter being the dominant component. Because of the complexity of the general expression for $\Delta(\mathbf{r}_1, \mathbf{r}_2, L)$ [see Eq. (39)], we begin by considering the limiting cases of plane wave and spherical wave.

6.4.1 Plane wave

The WSF associated with an *unbounded plane wave*, obtained from (39) by setting $\Theta = 1$ and $\Lambda = 0$, is given by

$$\begin{aligned} D_{\mathrm{pl}}(\rho, L) &= \mathrm{Re}[\Delta(\mathbf{r}_1, \mathbf{r}_2, L)] \\ &= 8\pi^2 k^2 L \int_0^\infty \kappa \Phi_n(\kappa)[1 - J_0(\kappa\rho)]\, d\kappa. \end{aligned} \tag{58}$$

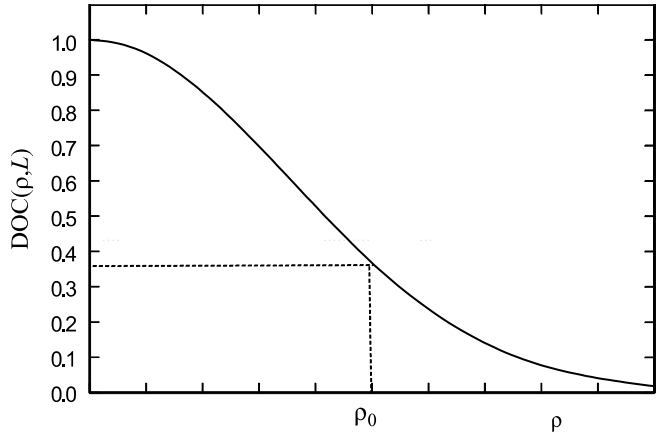

Figure 6.2 The DOC plotted as a function of separation distance, illustrating the spatial coherence radius ρ_0.

By expanding the Bessel function in a power series, we can write the WSF in the form

$$D_{\rm pl}(\rho, L) = 8\pi^2(0.033)C_n^2 k^2 L \sum_{n=1}^{\infty} \frac{(-1)^{n-1}\rho^{2n}}{2^{2n}(n!)^2} \int_0^{\infty} \frac{\kappa^{2n+1} \exp(-\kappa^2/\kappa_m^2)}{(\kappa^2 + \kappa_0^2)^{11/6}}\, d\kappa, \quad (59)$$

where we have used the von Kármán spectrum (28) and interchanged the order of summation and integration. Based on integral #17 in Appendix II and the asymptotic relation (CH8) in Appendix I, it can be shown that this last expression reduces to (see Prob. 16)

$$D_{\rm pl}(\rho, L) = 1.303C_n^2 k^2 L \left\{ \Gamma(-5/6)\kappa_m^{-5/3} \left[1 - {}_1F_1\left(-\frac{5}{6}; 1; -\frac{\kappa_m^2\rho^2}{4} \right) \right] - \frac{9}{5}\kappa_0^{1/3}\rho^2 \right\}. \quad (60)$$

It has been shown by Andrews et al. [20] that the confluent hypergeometric function in (60) can be accurately approximated ($<2\%$ error) by the algebraic term

$${}_1F_1\left(-\frac{5}{6}; 1; -x \right) - 1 \cong \frac{5x}{6}(1 + 0.232x)^{-1/6}, \qquad x \geq 0. \quad (61)$$

Thus, with only a minor error, Eq. (60) can be replaced by the simpler expression

$$D_{\rm pl}(\rho, L) = 3.28C_n^2 k^2 L l_0^{-1/3} \rho^2 \left[\frac{1}{(1 + 2.03\rho^2/l_0^2)^{1/6}} - 0.72(\kappa_0 l_0)^{1/3} \right]. \quad (62)$$

Comparable expressions based on the modified atmospheric spectrum [see Eq. (22) in Chap. 3] are provided in Ref. [20] and in Table I of Appendix III.

In many cases of interest, it suffices to know the form of the WSF only in certain asymptotic regimes. For example, from either (60) or (62) it is readily shown that

$$D_{\rm pl}(\rho, L) = \begin{cases} 3.28C_n^2 k^2 L l_0^{-1/3} \rho^2 \left[1 - 0.72(\kappa_0 l_0)^{1/3} \right], & \rho \ll l_0, \\ 2.91C_n^2 k^2 L \rho^{5/3} \left[1 - 0.81(\kappa_0 \rho)^{1/3} \right], & \rho \gg l_0. \end{cases} \quad (63)$$

Based on expressions given in (63), the implied *plane-wave spatial coherence radius* for the case $L_0 = \infty$ (i.e., $\kappa_0 = 0$) is

$$\rho_0 \equiv \rho_{\rm pl} = \begin{cases} (1.64C_n^2 k^2 L l_0^{-1/3})^{-1/2}, & \rho_{\rm pl} \ll l_0, \\ (1.46C_n^2 k^2 L)^{-3/5}, & l_0 \ll \rho_{\rm pl} \ll L_0, \end{cases} \qquad [\text{m}] \quad (64)$$

In some application areas, however, it is customary to define spatial coherence by the related *atmospheric coherence width* $r_0 = 2.1\rho_0$ (see Chaps. 12 and 14).

The structure functions for the log amplitude χ and phase S appearing in Eq. (57) are defined in the case of a plane wave by

$$D_{\chi,S}(\rho, L) = 4\pi^2 k^2 L \int_0^1 \int_0^{\infty} \kappa \Phi_n(\kappa)[1 - J_0(\kappa\rho)] \left[1 \mp \cos\left(\frac{L\kappa^2\xi}{k} \right) \right] d\kappa\, d\xi, \quad (65)$$

where the upper sign corresponds to the log amplitude and the lower sign to the phase. It has been shown that the *phase structure function* in various regimes reduces to

$$D_S(\rho, L) = \begin{cases} 1.64 C_n^2 k^2 L l_0^{-1/3} \left[1 + 0.64 (k l_0^2/L)^{1/6}\right] \rho^2, & \rho \ll l_0, \\ 1.46 C_n^2 k^2 L \rho^{5/3}, & l_0 \ll \rho \ll \sqrt{L/k}, \\ 2.91 C_n^2 k^2 L \rho^{5/3}, & \sqrt{L/k} \ll \rho \ll L_0. \end{cases} \tag{66}$$

Note that, for separation distances much greater than the first Fresnel zone but much smaller than the outer scale, the phase structure function is the same as the WSF. That is, under the geometrical optics approximation $L\kappa^2/k \ll 1$, we can write $\cos(L\kappa^2\xi/k) \cong 1$ and, therefore, $D_\chi(\rho, L) \cong 0$ and $D_S(\rho, L) \cong D_{\text{pl}}(\rho, L)$.

6.4.2 Spherical wave

The WSF for a *spherical wave* can also be determined from Eq. (39). In particular, by setting $\Theta = \Lambda = 0$, the real part of Eq. (39) leads to

$$D_{\text{sp}}(\rho, L) = 8\pi^2 k^2 L \int_0^1 \int_0^\infty \kappa \Phi_n(\kappa) [1 - J_0(\kappa \xi \rho)] \, d\kappa \, d\xi, \tag{67}$$

which, based on the von Kármán spectrum, reduces to [20] (see Prob. 19)

$$\begin{aligned} D_{\text{sp}}(\rho, L) = 1.303 C_n^2 k^2 L \Bigg\{ & \Gamma(-5/6) \kappa_m^{-5/3} \\ & \times \left[1 - {}_2F_2\left(-\frac{5}{6}, \frac{1}{2}; 1, \frac{3}{2}; -\frac{\kappa_m^2 \rho^2}{4} \right) \right] - \frac{3}{5} \kappa_0^{1/3} \rho^2 \Bigg\}, \end{aligned} \tag{68}$$

where ${}_2F_2$ denotes a generalized hypergeometric function (see Appendix I).

Similar to the plane wave case, the WSF (68) can be closely approximated by the simple algebraic expression

$$D_{\text{sp}}(\rho, L) = 1.09 C_n^2 k^2 L l_0^{-1/3} \rho^2 \left[\frac{1}{\left(1 + \rho^2/l_0^2\right)^{1/6}} - 0.72 (\kappa_0 l_0)^{1/3} \right]. \tag{69}$$

A comparable result based on the modified atmospheric spectrum is provided in Ref. [20] and in Table II of Appendix III. Asymptotic formulas deduced from either (68) or (69) are given by

$$D_{\text{sp}}(\rho, L) = \begin{cases} 1.09 C_n^2 k^2 L l_0^{-1/3} \rho^2 \left[1 - 0.72 (\kappa_0 l_0)^{1/3}\right], & \rho \ll l_0, \\ 1.09 C_n^2 k^2 L \rho^{5/3} \left[1 - 0.72 (\kappa_0 \rho)^{1/3}\right], & \rho \gg l_0. \end{cases} \tag{70}$$

By taking the special case $L_0 = \infty$ (i.e., $\kappa_0 = 0$), it follows that the *spherical-wave spatial coherence radius* deduced from (70) is

$$\rho_0 \equiv \rho_{\text{sp}} = \begin{cases} (0.55C_n^2 k^2 L l_0^{-1/3})^{-1/2}, & \rho_{\text{sp}} \ll l_0, \\ (0.55C_n^2 k^2 L)^{-3/5}, & l_0 \ll \rho_{\text{sp}} \ll L_0. \end{cases} \quad [\text{m}] \tag{71}$$

The structure functions for the log amplitude χ and phase S appearing in Eq. (57) are defined in the case of a spherical wave by

$$D_{\chi,S}(\rho, L) = 4\pi^2 k^2 L \int_0^1 \int_0^\infty \kappa \Phi_n(\kappa)[1 - J_0(\kappa\xi\rho)] \times \left\{1 \mp \cos\left[\frac{L\kappa^2}{k}\xi(1-\xi)\right]\right\} d\kappa\, d\xi, \tag{72}$$

where the upper sign corresponds to the log amplitude and the lower sign to the phase. If we examine the limit of the geometrical optics approximation in this case, we will conclude that the log-amplitude structure function is essentially zero and, hence, the WSF reduces to the phase structure function as in the plane wave case.

6.4.3 Gaussian-beam wave

The WSF associated with a Gaussian-beam wave defined by the real part of Eq. (39) is statistically inhomogeneous in that it depends on the position of the two observation points $\mathbf{r}_1$ and $\mathbf{r}_2$. However, for the special case $\mathbf{r}_2 = -\mathbf{r}_1$ the WSF takes the simpler form

$$D(\rho, L) = 8\pi^2 k^2 L \int_0^1 \int_0^\infty \kappa \Phi_n(\kappa) \exp\left(-\frac{\Lambda L \kappa^2 \xi^2}{k}\right) \times \{I_0(\Lambda\rho\xi\kappa) - J_0\left[\left(1 - \overline{\Theta}\xi\right)\kappa\rho\right] d\kappa\, d\xi\}, \tag{73}$$

which, for $l_0 \ll \rho \ll L_0$, we recognize as

$$D(\rho, L) = d(\rho, L) + 4\sigma_r^2(\rho/2, L) \cong 1.09C_n^2 k^{7/6} L^{11/6}\left[a\left(\frac{k\rho^2}{L}\right)^{5/6} + 0.62\Lambda^{11/6}\left(\frac{k\rho^2}{L}\right)\right], \qquad l_0 \ll \rho \ll L_0, \tag{74}$$

where a is defined by (55). To obtain a more general form involving the inner scale and outer scale, we illustrate with the von Kármán spectrum (28). The evaluation of (73) in this case leads to [17]

$$D(\rho, L) \cong 1.09C_n^2 k^2 L l_0^{-1/3} \rho^2 g(\rho, L), \tag{75}$$

where $g(\rho, L)$ can be approximated by

$$g(\rho, L) = \frac{\Lambda^2}{(1 + 0.52\Lambda Q_m)^{1/6}} - 0.72(1 + \Theta + \Theta^2 + \Lambda^2)(\kappa_0 l_0)^{1/3} + \frac{1}{(1 - \Theta)} \times \left[\frac{1}{\left(1 + 0.11\Lambda Q_m + \rho^2/l_0^2\right)^{1/6}} - \frac{\Theta^3}{\left(1 + 0.11\Lambda Q_m + \Theta^2\rho^2/l_0^2\right)^{1/6}} \right]. \tag{76}$$

When the separation distance is either very small or very large in comparison with the size of the inner scale, the WSF (75) simplifies to one of the asymptotic forms

$$D(\rho, L) \cong \begin{cases} 1.09 C_n^2 k^2 L l_0^{-1/3} \rho^2 (1 + \Theta + \Theta^2 + \Lambda^2)\left[1 - 0.72(\kappa_0 l_0)^{1/3}\right], & \rho \ll l_0, \\ 1.09 C_n^2 k^{7/6} L^{11/6} \left[a \left(\dfrac{k\rho^2}{L} \right)^{5/6} + 0.62\Lambda^{11/6} \left(\dfrac{k\rho^2}{L} \right) \right. \\ \qquad \left. - 0.72(1 + \Theta + \Theta^2 + \Lambda^2)(\kappa_0 \rho)^{1/3} \left(\dfrac{k\rho^2}{L} \right)^{5/6} \right], & \rho \gg l_0. \end{cases} \tag{77}$$

Note that relations (77) reduce to Eqs. (63) and (70), respectively, in the plane wave limit ($\Theta = 1$, $\Lambda = 0$) and spherical wave limit ($\Theta = \Lambda = 0$).

The WSF based on the modified atmospheric spectrum is given in Ref. [19] and also in Table III of Appendix III. To illustrate the effect of the bump in this spectrum model, we show the WSF in Fig. 6.3 as a function of ρ/l_0 for two collimated beams. The solid curves depict results as predicted by the modified atmospheric spectrum and the dashed curves represent the Tatarskii spectrum [Eq. (19) in

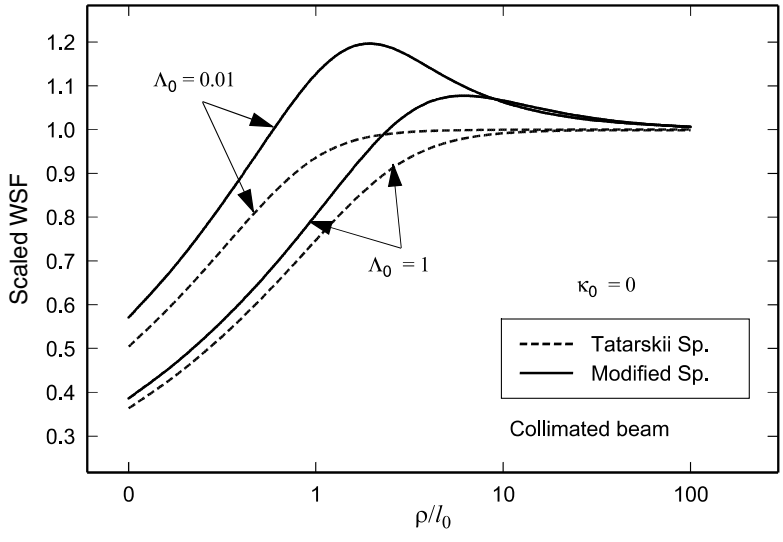

Figure 6.3 The WSF (75), scaled by the inertial range form (74), of two collimated beams as a function of ρ/l_0. The outer scale is assumed infinite.

Chap. 3], both scaled by the inertial range form (77) with $\kappa_0 = 0$ and $\rho \ll l_0$. Here we clearly see that the bump in the spectrum produces a corresponding bump in the WSF near separation distances for which $\rho/l_0 \sim 2$ to 5.

The spatial coherence radius ρ_0 is harder to deduce from Eq. (77) for a Gaussian-beam wave than corresponding expressions for plane waves and spherical waves. However, with $\kappa_0 = 0$ and the approximation $(k\rho^2/L) \cong (k\rho^2/L)^{5/6}$ for $\rho \gg l_0$, it follows that when the *spatial coherence radius* is either much smaller or much larger than the inner scale size, it can be approximated by the relatively simple asymptotic expressions

$$\rho_0 = \begin{cases} \left(\dfrac{3}{1+\Theta+\Theta^2+\Lambda^2}\right)^{1/2} \left(1.64 C_n^2 k^2 L l_0^{-1/3}\right)^{-1/2}, & \rho_0 \ll l_0 \\ \left[\dfrac{8}{3\left(a+0.62\Lambda^{11/6}\right)}\right]^{3/5} (1.46 C_n^2 k^2 L)^{-3/5}, & l_0 \ll \rho_0 \ll L_0. \end{cases} \quad \text{[m]} \quad (78)$$

Clearly, in the plane wave and spherical wave limits, Eq. (78) reduces to the corresponding expressions given in Eqs. (64) and (71), respectively.

In Fig. 6.4, the ratio of coherence radii ρ_0/ρ_{pl} deduced from Eq. (78) for a collimated beam ($\Theta_0 = 1$) and $l_0 \ll \rho_0 \ll L_0$ is shown as a function of Fresnel ratio Λ_0. For $\Lambda_0 \ll 1$ (near field), the ratio is essentially unity, illustrating that the coherence radius of the Gaussian-beam wave is approximately that of a plane wave. On the other hand, the coherence radius of a collimated beam approaches that of a spherical wave for $\Lambda_0 \gg 1$ (far field), but in general lies between the plane wave and spherical wave limits.

The lower equation in (78) for the coherence radius of a Gaussian-beam wave with $l_0 \ll \rho_0 \ll L_0$ is valid in the inertial subrange under all spectral models.

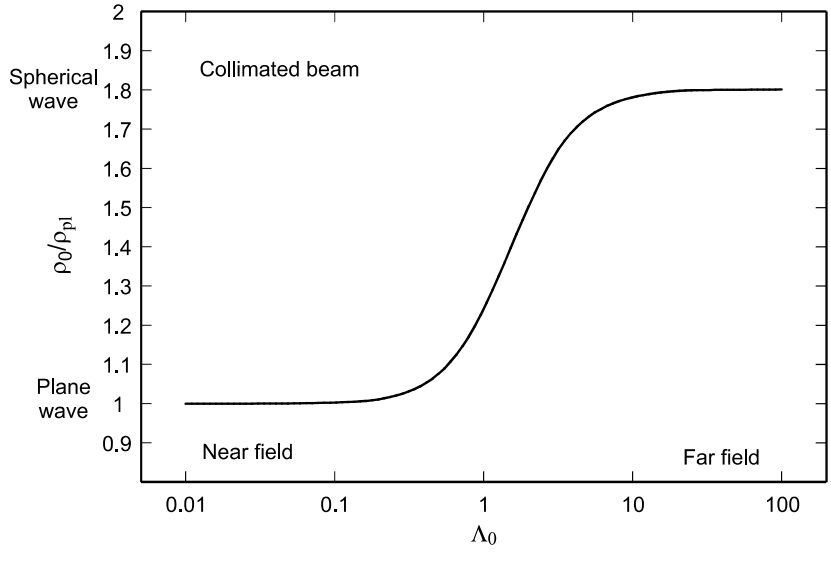

Figure 6.4 Spatial coherence radius ρ_0 of a collimated Gaussian-beam wave, scaled by the plane wave coherence radius ρ_{pl} and plotted as a function of Fresnel ratio Λ_0.

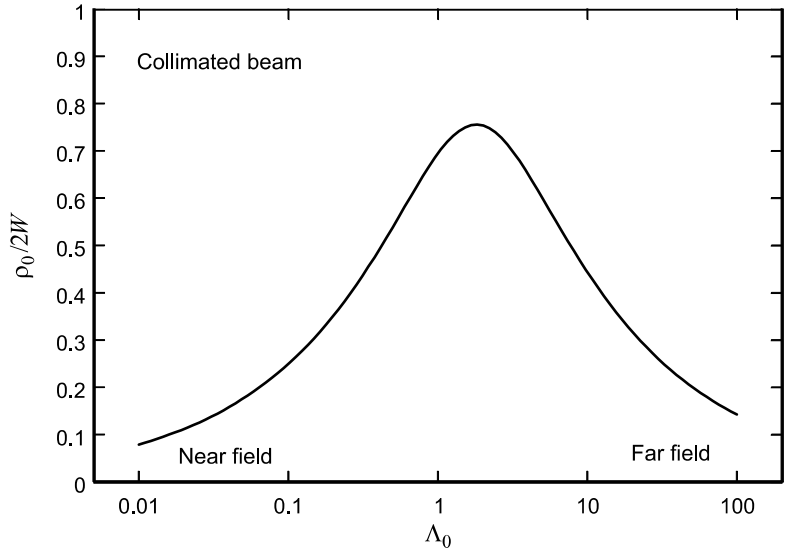

Figure 6.5 Spatial coherence radius ρ_0 of a collimated Gaussian-beam wave, scaled by the diffractive beam diameter and plotted as a function of Fresnel ratio Λ_0. The assumed turbulence strength is $q = 0.2$.

However, as the coherence radius decreases in size below that of the inner scale, deviations away from the inertial range form depend upon the choice of spectral model. The asymptotic form given in Eq. (78) for the case $\rho_0 \ll l_0$ is based on the von Kármán spectrum [17]. For the modified atmospheric spectrum with $\rho_0 \ll l_0$, the implied spatial coherence radius is generally less than that predicted by the von Kármán spectrum [19] (see also Tables IV–VI in Appendix III).

A different perspective of coherence radius is observed by considering the ratio of coherence radius and diffractive beam diameter. Within the inertial subrange, this ratio is described by

$$\frac{\rho_0}{2W} = 0.35\left(\frac{\Lambda}{q}\right)^{1/2}\left[\frac{8}{3(a + 0.62\Lambda^{11/6})}\right]^{3/5}, \qquad l_0 \ll \rho_0 \ll L_0, \tag{79}$$

where $q = 1.22(\sigma_R^2)^{6/5}$. The ratio (79) is plotted in Fig. 6.5 for a collimated beam as a function of beam size Λ_0 and $q = 0.2$. Here we see that, for a fixed value of turbulence strength q, the largest ratio of coherence radius to beam diameter occurs for those beams in which $\Lambda_0 \sim 1$ to 3.

6.5 Angle-of-Arrival Fluctuations

Having derived a model for the MCF, there are related statistical quantities that are readily deduced from this expression that have important consequences on beam wave propagation applications such as imaging, lasercom, laser radar, and so

on. In this section we examine angle-of-arrival fluctuations, and in the next section we present models for beam wander and the short-term beam radius.

Angle-of-arrival fluctuations of an optical wave in the plane of the receiver aperture are associated with image jitter (dancing) in the focal plane of an imaging system. Fluctuations in the angle of arrival β_a can be described in terms of the phase structure function. To understand this, let ΔS denote the total phase shift across a collecting lens of diameter $2W_G$ and Δl the corresponding optical path difference. These quantities are related by

$$k\Delta l = \Delta S. \tag{80}$$

If we assume that β_a is small so that $\sin\beta_a \cong \beta_a$ (see Fig. 6.6), then, under the *geometrical optics method* (GOM), the angle of arrival is defined by [2,3]

$$\beta_a = \frac{\Delta l}{2W_G} = \frac{\Delta S}{2kW_G}. \quad \text{[radian]} \tag{81}$$

Further assuming the mean $\langle\beta_a\rangle = 0$, we deduce the *variance of the angle of arrival*

$$\langle\beta_a^2\rangle = \frac{\langle(\Delta S)^2\rangle}{(2kW_G)^2} = \frac{D_S(2W_G, L)}{(2kW_G)^2}, \tag{82}$$

where $D_S(\rho, L)$ is the phase structure function. In the case of a plane wave and Kolmogorov spectrum, Eq. (82) reduces (roughly) to

$$\langle\beta_a^2\rangle = \begin{cases} 1.64C_n^2 L l_0^{-1/3}\left[1 - 0.72(\kappa_0 l_0)^{1/3}\right], & 2W_G \ll l_0 \\ 2.91C_n^2 L(2W_G)^{-1/3}\left[1 - 0.81(2\kappa_0 W_G)^{1/3}\right], & 2W_G \gg l_0, \end{cases} \tag{83}$$

where we have approximated the phase structure function by the WSF and included the effects of both inner and outer scale. Notice that (83) is independent of optical wavelength—however, this is true only if the Fresnel zone is sufficiently small compared with the receiver aperture diameter, i.e., $\sqrt{L/k} \ll 2W_G$. For a spherical wave or Gaussian-beam wave, similar expressions can be deduced

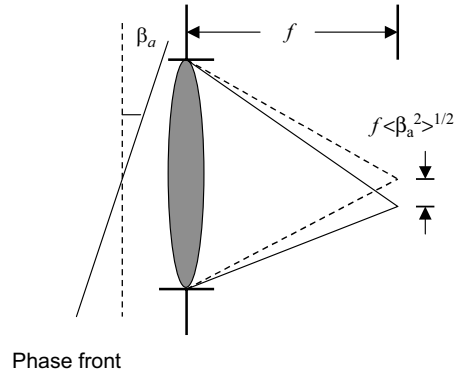

Figure 6.6 Angle of arrival and image jitter.

from the WSFs given by Eqs. (70) and (77). Although the mean angle-of-arrival, or tilt angle, is zero, it is useful to introduce the notion of the *root-mean-square* (*rms*) *angle-of-arrival*, defined by (now ignoring inner scale and outer-scale effects for mathematical simplicity)

$$\sqrt{\langle \beta_a^2 \rangle} = \sqrt{2.91 C_n^2 L (2W_G)^{-1/3}}, \qquad 2W_G \gg l_0. \tag{84}$$

The theoretical approach to *image jitter* is the same as that above for tilt or angle-of-arrival fluctuations except it takes place in the focal plane of the system (see Fig. 6.6). That is, the *rms image displacement* is the rms angle of arrival multiplied by the focal length f of the collecting lens of the receiver. For example, using (83), we write

$$\text{rms image jitter} = \begin{cases} f\sqrt{1.64 C_n^2 L l_0^{-1/3}\left[1 - 0.72(\kappa_0 l_0)^{1/3}\right]}, & 2W_G \ll l_0 \\ f\sqrt{2.91 C_n^2 L (2W_G)^{-1/3}\left[1 - 0.81(2\kappa_0 W_G)^{1/3}\right]}, & 2W_G \gg l_0. \end{cases} \tag{85}$$

6.6 Beam Wander

The far-field angular spread of a free-space propagating laser beam of diameter $2W_0$ is of order $\lambda/2W_0$. In the presence of optical turbulence, however, a finite optical beam will experience random deflections as it propagates, causing further spreading of the beam by large-scale inhomogeneities of the atmosphere. Over short time periods the beam profile at the receiver randomly moves off the boresight and, in doing so, can become highly skewed from Gaussian (see Fig. 6.7). The *instantaneous center* of the beam (point of maximum irradiance or "hot spot") is therefore randomly displaced in the receiver plane, producing what is commonly called *beam wander* [21–31]. This phenomenon can be characterized statistically by the variance of the hot spot displacement along an axis or by the variance of the magnitude of the hot spot displacement. Beam wander has a time constant on the order of (beam diameter)/(wind speed), and thus it can be canceled with the use of a fast-tracking transmitter.

It is known that beam wander is caused mostly by large-scale turbulence near the transmitter, and for that reason the analysis is often based on the GOM, where diffraction effects are neglected. Chernov [22] and Beckmann [23] both used the GOM in their analyses, but did not consider the finite size of the beam. Chiba [25] included the finite size of the beam in his analysis for the case of a collimated beam, and Churnside and Lataitis [21] used the GOM to develop an expression for the variance of the beam wander displacement that included both collimated and focused beams. A more comprehensive analysis of beam wander that includes diffraction effects has also been developed by using the Markov approximation [26,30,31]. In this latter approach, the analysis led to the introduction of a spatial filter that suppresses the influence of turbulent eddy sizes smaller than the beam. Fante [6] developed a relation between the long-term beam spot

size, the short-term beam spot size, and the variance of displacement of the short-term beam using fourth-order statistics. Tavis and Yura [32] also developed a short-term beam profile, but their analysis was based on the small-scale effect of turbulence.

6.6.1 A general model

Beam wander at the receiver plane can be modeled as if it arises from a random tilt angle at the transmitter plane, similar to angle-of-arrival fluctuations of a reciprocal propagating wave with the receiver diameter replaced by the transmitter beam diameter. The movement of the short-term beam depicted by the shaded circular regions in Fig. 6.7(*b*) leads to the large outer circle over a long time period that we call the long-term spot size W_{LT}. To develop an analytic expression for the variance of beam wander fluctuations, we will use the long-term spot size (46), the square of which yields

$$W_{\mathrm{LT}}^2 = W^2(1+T) = W^2\left(1 + 1.33\sigma_R^2\Lambda^{5/6}\right). \tag{86}$$

Based on the concept of short- and long-term spot size, we now write this as

$$W_{\mathrm{LT}}^2 = \underbrace{W^2}_{\substack{\textbf{diffrac.}}} + \underbrace{W^2 T_{\mathrm{SS}}}_{\substack{\textbf{sm-scale}\\ \textbf{spread}}} + \underbrace{W^2 T_{\mathrm{LS}}}_{\substack{\textbf{large-scale}\\ \textbf{beamwander}}}, \tag{87}$$

where we have partitioned the term $T = T_{\mathrm{SS}} + T_{\mathrm{LS}}$ into a sum of small-scale (SS) and large-scale (LS) contributions. Doing so, we can interpret the first term in (87) as that due to pure diffraction spreading, the first and middle terms as that defining

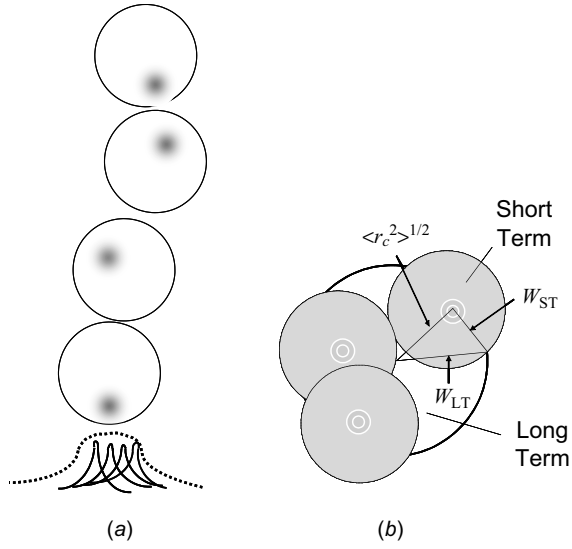

Figure 6.7 (*a*) Beam wander as described by movement of the "hot spot" (instantaneous center) within the beam. (*b*) The long-term spot size is the result of beam wander, beam breathing, and diffraction. The shaded circles depict random motion of the short-term beam in the receiver plane.

"beam breathing" and the short-term beam radius W_{ST}, and the last term as that describing "beam wander" or the variance of the instantaneous center of the beam in the receiver plane ($z = L$). Because it arises from large-scale turbulence, we model the last term by the expression

$$\langle r_c^2 \rangle = W^2 T_{\mathrm{LS}} = 4\pi^2 k^2 W^2 \int_0^L \int_0^\infty \kappa \Phi_n(\kappa) H_{\mathrm{LS}}(\kappa, z) \left(1 - e^{-\Lambda L \kappa^2 \xi^2 / k}\right) d\kappa \, dz, \quad (88)$$

where $\xi = 1 - z/L$ and we have introduced the large-scale filter function [26,30,31]

$$H_{\mathrm{LS}}(\kappa, z) = \exp\left[-\kappa^2 W^2(z)\right] = \exp\left\{-\kappa^2 W_0^2 \left[(1 - z/F_0)^2 + (2z/kW_0^2)^2\right]\right\}. \quad (89)$$

The Gaussian filter function (89) only permits random inhomogeneities equal to the beam size and larger to contribute to beam wander, thereby eliminating small-scale effects that lead to the second term in (87). In (89), $W(z)$ is the free-space beam radius at variable distance $z\,(0 < z < L)$ from the transmitter. Of course, the outer scale of turbulence L_0 forms an upper bound on the inhomogeneity size that can cause beam wander [33]. Inner scale effects are negligible here so we only include the outer scale parameter in our spectrum model. In our analysis we will introduce outer scale effects through use of the exponential spectrum model (Section 3.3.2)

$$\Phi_n(\kappa) = 0.033 C_n^2 \kappa^{-11/3} \left[1 - \exp\left(-\frac{\kappa^2}{\kappa_0^2}\right)\right], \qquad \kappa_0 = \frac{C_0}{L_0}. \quad (90)$$

The scaling constant C_0 for the outer scale parameter κ_0 in (90) is typically chosen in the range $1 \le C_0 \le 8\pi$ (see Fig. 3.8).

For integration purposes, we will use the normalized distance variable $\xi = 1 - z/L$ along with the input plane beam parameters Θ_0 and Λ_0 to write the filter function (89) in the more convenient form

$$H_{\mathrm{LS}}(\kappa, \xi) = \exp\left\{-\kappa^2 W_0^2 \left[\left(\Theta_0 + \overline{\Theta}_0 \xi\right)^2 + \Lambda_0^2 (1 - \xi)^2\right]\right\}. \quad (91)$$

To emphasize the refractive nature of beam wander, we will also drop the last term in (91) and use the geometrical optics approximation

$$1 - e^{-\Lambda L \kappa^2 \xi^2 / k} \cong \frac{\Lambda L \kappa^2 \xi^2}{k}, \qquad L\kappa^2/k \ll 1. \quad (92)$$

In this case Eq. (88) leads to

$$\begin{aligned} \langle r_c^2 \rangle &= 1.303 C_n^2 k L^2 W^2 \Lambda \int_0^1 \xi^2 \int_0^\infty \kappa^{-2/3} \left[1 - \exp\left(-\frac{\kappa^2}{\kappa_0^2}\right)\right] \\ &\quad \times \exp\left[-\kappa^2 W_0^2 (\Theta_0 + \overline{\Theta}_0 \xi)^2\right] d\kappa \, d\xi \quad (93) \\ &= 7.25 C_n^2 L^3 W_0^{-1/3} \int_0^1 \xi^2 \left\{ \frac{1}{|\Theta_0 + \overline{\Theta}_0 \xi|^{1/3}} - \left[\frac{\kappa_0^2 W_0^2}{1 + \kappa_0^2 W_0^2 \left(\Theta_0 + \overline{\Theta}_0 \xi\right)^2}\right]^{1/6} \right\} d\xi. \end{aligned}$$

Equation (93) is applicable for collimated, divergent, or convergent (focused) Gaussian-beam waves, and thus represents our general expression for the *variance*

of beam wander displacement under weak irradiance fluctuations and constant C_n^2. The second term under the integral represents the limiting effects of a finite outer scale on the overall beam wander variance.

6.6.2 Special cases

For the case of an *infinite outer scale* ($\kappa_0 = 0$), the remaining integral in (93) yields

$$\langle r_c^2 \rangle = 2.42 C_n^2 L^3 W_0^{-1/3} \, {}_2F_1\left(\frac{1}{3}, 1; 4; 1 - |\Theta_0|\right). \tag{94}$$

Equation (94) emphasizes the close connection between beam wander in the receiver plane and the tilt angle variance $\langle \beta_a^2 \rangle$ at the transmitter of a reciprocal propagating plane wave [e.g., see (83) or (84)]. When the beam parameter Θ_0 in (94) satisfies $\Theta_0 \geq 0$ (i.e., collimated, divergent, and convergent beam cases in which $F_0 \geq L$), the absolute value signs are not necessary. Except for a small difference in the constant, Eq. (94) is the same result as that obtained by Churnside and Lataitis [21] using the GOM. For a *collimated beam* ($\Theta_0 = 1$) the hypergeometric function in (94) is unity, and the expression reduces to

$$\text{Collimated beam } (\kappa_0 = 0): \qquad \langle r_c^2 \rangle = 2.42 C_n^2 L^3 W_0^{-1/3}, \tag{95}$$

from which we deduce $\langle r_c^2 \rangle \cong L^2 \langle \beta_a^2 \rangle$ by equating $W_G = W_0$. For a beam that is *focused* in the receiver plane ($\Theta_0 = 0$), the hypergeometric function is 1.13 and

$$\text{Focused beam } (\kappa_0 = 0): \qquad \langle r_c^2 \rangle = 2.72 C_n^2 L^3 W_0^{-1/3}. \tag{96}$$

Thus, the focused beam case leads to a somewhat greater beam-wander variance for the same size beam at the transmitter as that for the collimated beam.

When a finite outer scale is present ($\kappa_0 \neq 0$) and we consider a collimated beam ($\Theta_0 = 1$ and $\overline{\Theta}_0 = 0$), then in this case Eq. (93) reduces to

$$\text{Collimated beam } (\kappa_0 \neq 0): \qquad \langle r_c^2 \rangle = 2.42 C_n^2 L^3 W_0^{-1/3} \left[1 - \left(\frac{\kappa_0^2 W_0^2}{1 + \kappa_0^2 W_0^2} \right)^{1/6} \right]. \tag{97}$$

For a focused beam in the presence of a finite outer scale, we set $\Theta_0 = 0$ and $\overline{\Theta}_0 = 1$ in Eq. (93). The resulting integral yields

$$\langle r_c^2 \rangle = 2.72 C_n^2 L^3 W_0^{-1/3} \left[1 - \frac{8}{3} (\kappa_0 W_0)^{1/3} \int_0^1 \frac{\xi^2}{\left(1 + \kappa_0^2 W_0^2 \xi^2\right)^{1/6}} \, d\xi \right]. \tag{98}$$

Without significant loss of accuracy, we can further reduce (98) to the simple algebraic approximation

$$\text{Focused beam } (\kappa_0 \neq 0): \langle r_c^2 \rangle = 2.72 C_n^2 L^3 W_0^{-1/3} \left[1 - \frac{8}{9} \left(\frac{\kappa_0^2 W_0^2}{1 + 0.5 \kappa_0^2 W_0^2} \right)^{1/6} \right]. \tag{99}$$

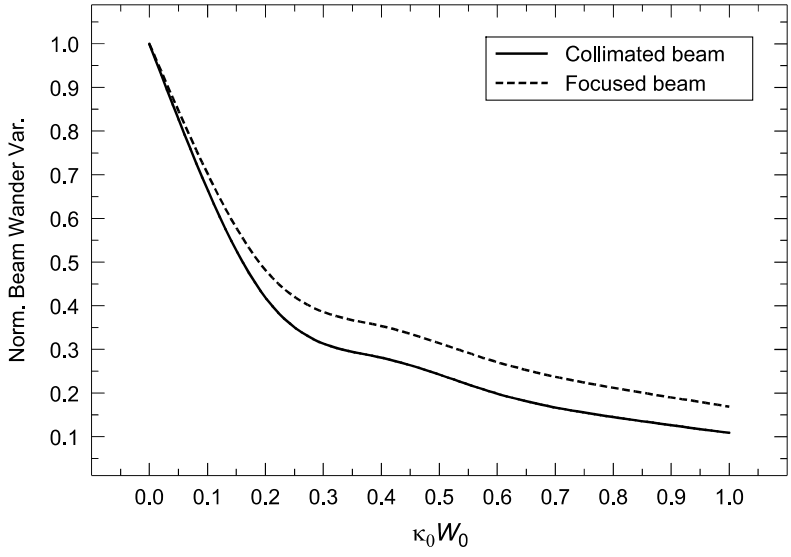

Figure 6.8 Ratio of beam wander variance with a finite outer scale to that with infinite outer scale. The solid curve corresponds to a collimated beam and the dashed curve to a focused beam.

Although often omitted in theoretical analyses, the presence of a finite outer scale can have a big effect on the amount of beam wander that actually occurs [33]. To illustrate this effect in the case of a collimated beam, we plot (97) in Fig. 6.8 scaled by (95), the latter for the case of an infinite outer scale. Initially, there is a significant drop in beam wander in the presence of outer scale and, as the transmitter beam size approaches the dimension of the outer scale ($\kappa_0 W_0 \sim 1$), the beam wander displacement nearly vanishes. In fact, even with $\kappa_0 W_0 = 0.1$, beam wander is less than 70% of that predicted with an infinite outer scale. We also show the normalized beam wander variance for a focused beam (dashed curve), obtained by taking the ratio of (99) and (96), the latter for the infinite outer-scale case. As in the case of a collimated beam, the rms wander of a focused beam can be greatly diminished in the presence of a finite outer scale.

6.6.3 Short-term beam spreading

The long-term beam spreading of a Gaussian beam is described by Eq. (86). If we denote the short-term beam radius by W_{ST}, then Fante's [6] relation between the long-term beam radius, short-term beam radius, and beam wander variance is given by (see Fig. 6.7)

$$W_{\mathrm{LT}}^2 = W_{\mathrm{ST}}^2 + \langle r_c^2 \rangle. \tag{100}$$

Note that Eq. (100) is equivalent to Eq. (87) where we can identify the short-term beam radius by the term $W_{\mathrm{ST}} = W\sqrt{1 + T_{\mathrm{SS}}}$. Consequently, based on Eqs. (95),

(96), and (100), the *short-term beam radius* for a collimated beam or focused beam in the case of an infinite outer scale can be written in the form

$$W_{\mathrm{ST}} = \begin{cases} W\sqrt{1 + 1.33\sigma_R^2\Lambda^{5/6}\left[1 - 0.66\left(\dfrac{\Lambda_0^2}{1+\Lambda_0^2}\right)^{1/6}\right]} & \text{(collimated beam)} \\ W\sqrt{1 + 0.35\sigma_R^2\Lambda^{5/6}} & \text{(focused beam).} \end{cases} \tag{101}$$

Based on (101), it is clear that the beam short-term spot size is always smaller than the long-term ensemble averaged spot size (86). In fact, under some weak fluctuation conditions, the short-term spot size is not much larger than the free-space spot size caused entirely by diffraction. Among other applications, the short-term beam is important in postprocessing techniques used to overcome atmospheric degradation effects in imaging.

6.7 Angular and Temporal Frequency Spectra

If the two-dimensional Fourier transform is applied to the complex field distribution at any point in free space, the various spatial Fourier components can be identified as plane waves traveling in different directions [34]. Hence, the field amplitude at any other point can be calculated by adding the contributions of these plane waves, taking into account the various phase shifts caused by propagation. We refer to such a Fourier transform as the *angular spectrum* of the field. For an optical field propagating through optical turbulence, it is the Fourier transform of the MCF that leads to the angular spectrum [7].

In the case of an infinite plane wave, the MCF (neglecting inner scale and outer scale effects) can be written as

$$\Gamma_2(\mathbf{p}, L) = \exp\left[-\left(\frac{\rho}{\rho_{\mathrm{pl}}}\right)^{5/3}\right], \tag{102}$$

where $\rho_{\mathrm{pl}} = (1.46C_n^2 k^2 L)^{-3/5}$. The angular spectrum is defined by

$$\begin{aligned} \hat{\Gamma}_2(\boldsymbol{\theta}, L) &= \frac{k^2}{(2\pi)^2}\int\int_{-\infty}^{\infty} \exp(-ik\mathbf{p}\cdot\boldsymbol{\theta})\Gamma_2(\mathbf{p}, L)\, d^2p \\ &= \frac{k^2}{2\pi}\int_0^{\infty} \rho J_0(k\rho\theta)\exp\left[-\left(\frac{\rho}{\rho_{\mathrm{pl}}}\right)^{5/3}\right] d\rho. \end{aligned} \tag{103}$$

The complexity of (103) does not permit simple evaluation, but we can rewrite it in the form

$$\hat{\Gamma}_2(\theta, L) = \frac{1}{2\pi\theta_c^2}\int_0^{\infty} sJ_0(\theta s/\theta_c)\exp(-s^{5/3})\, ds, \tag{104}$$

where $\theta_c = 1/(k\rho_{\mathrm{pl}})$. Although Eq. (104) is in a convenient form for numerical evaluation, we can make the approximation $s^{5/3} \cong s^2$ and directly evaluate the

resulting integral (see #11 in Appendix II). Consequently, the scaled angular spectrum can be reasonably approximated by the simple Gaussian function

$$\frac{\hat{\Gamma}_2(\theta, L)}{\hat{\Gamma}_2(0, L)} = \exp\left(-\frac{\theta^2}{4\theta_c^2}\right), \tag{105}$$

from which we deduce the width of the angular spectrum is roughly $2\theta_c = \lambda/\pi\rho_{\text{pl}}$.

In some applications it is also important to know the temporal frequency spectrum. That is, optical turbulence will cause a certain amount of frequency spreading around the carrier frequency ω_0 of a monochromatic wave. The MCF combined with the *Taylor frozen turbulence hypothesis* (Section 3.4) permits us to make such calculations.

To illustrate the approach, we will again restrict the analysis here to that of an infinite plane wave. If the mean transverse wind velocity component is designated by $\mathbf{V}_\perp$, then the frozen turbulence hypothesis permits us to make the association between spatial separation $\mathbf{p}$ and the transverse wind velocity, which in the case of an infinite plane wave is simply $\mathbf{p} = \mathbf{V}_\perp\tau$. The *temporal frequency spectrum* is then defined by

$$\begin{aligned} W(\omega, L) &= 2\int_{-\infty}^{\infty} \exp(-i\omega\tau)\Gamma_2(\mathbf{V}_\perp\tau, L)d\tau \\ &= \frac{2}{\omega_c}\int_{-\infty}^{\infty} \exp(-i\omega s/\omega_c)\exp\left(-s^{5/3}\right)ds, \end{aligned} \tag{106}$$

where $\omega_c = V_\perp/\rho_{\text{pl}}$. As in the angular spectrum, we can make the approximation $s^{5/3} \cong s^2$ and directly evaluate the resulting integral. Doing so yields the Gaussian approximation for the normalized frequency spectrum (106) given by

$$\frac{W(\omega, L)}{W(0, L)} \cong \exp\left(-\frac{\omega^2}{4\omega_c^2}\right), \tag{107}$$

where $\omega_0 \pm 2\omega_c$ identifies the frequency spread around the carrier frequency.

6.8 Slant Paths

Up to this point we have only considered the case of horizontal propagation paths for which the refractive-index structure parameter C_n^2 can be taken as constant. When this parameter varies along the propagation path, such as that associated with a *slant path*, then we must modify our expressions developed above for beam spot size, spatial coherence radius, and so on, to account for such variations. In particular, propagation paths between a point on or near the ground and an elevated point such as a mountain top or airborne platform, the structure parameter can be expressed as a function of altitude h. Several $C_n^2(h)$ profile models have been developed over the years, some of which are introduced in Chap. 12. These $C_n^2(h)$ profile models permit the user to make calculations for various slant path propagation channels as suggested above. Consequently, the statistical results presented here can be readily generalized to a variety of other propagation path

environments. In Chap. 12 we will further use such models to explore the case of propagation from ground/aircraft to a satellite in space, and from space to ground and/or airborne platforms.

6.8.1 Mean irradiance

A general expression for the *mean irradiance* is provided by Eq. (40). However, the expressions for $\sigma_r^2(\mathbf{r}, L)$ and T given by (42) and (43), respectively, will now take on a somewhat different form. In particular, here we find that

$$\begin{aligned}\sigma_r^2(\mathbf{r}, L) &= 2\pi^2 k^2 \int_0^L \int_0^\infty \kappa \Phi_n(\kappa, z) \exp\left[-\frac{\Lambda L \kappa^2 (1 - z/L)^2}{k}\right] \\ &\quad \times \left\{I_0[2\Lambda r \kappa (1 - z/L)] - 1\right\} d\kappa\, dz \\ &= 3.62 k^{7/6} L^{5/6} \Lambda^{5/6} \frac{r^2}{W^2} \int_0^L C_n^2(z)(1 - z/L)^{5/3} dz, \end{aligned} \tag{108}$$

$$\begin{aligned} T &= 4\pi^2 k^2 \int_0^L \kappa \Phi_n(\kappa, z) \left\{1 - \exp\left[-\frac{\Lambda L \kappa^2 (1 - z/L)^2}{k}\right]\right\} d\kappa\, dz \\ &= 4.35 k^{7/6} L^{5/6} \Lambda^{5/6} \int_0^L C_n^2(z)(1 - z/L)^{5/3}\, dz, \end{aligned} \tag{109}$$

where we have assumed a Kolmogorov spectrum

$$\Phi_n(\kappa, z) = 0.033 C_n^2(z) \kappa^{-11/3}. \tag{110}$$

If we now invoke the same kind of approximation that led to the Gaussian form (45), the resulting long-term beam radius based on (109) is given by

$$W_{\mathrm{LT}} \cong W \sqrt{1 + 4.35 k^{7/6} L^{5/6} \Lambda^{5/6} \int_0^L C_n^2(z)(1 - z/L)^{5/3}\, dz}. \tag{111}$$

Naturally, the results can be generalized to include other spectrum models featuring inner scale and outer scale parameters but these cases lead to more complicated expressions. Moreover, they require knowledge of the dependency of inner and outer scale on propagation distance and/or altitude (which is still generally unknown).

6.8.2 Spatial coherence

The *wave structure function* for an infinite plane wave is defined by (58) under general conditions. Using the Kolmogorov spectrum (110), we find that the only quantity in (58) that depends on the path variable z is the structure parameter. Hence, we readily deduce in this case that

$$D_{\mathrm{pl}}(\rho, L) = 2.91 k^2 \rho^{5/3} \int_0^L C_n^2(z)\, dz, \qquad l_0 \ll \rho_{\mathrm{pl}} \ll L_0, \tag{112}$$

from which we obtain

$$\rho_{\mathrm{pl}} = \left[1.46k^2 \int_0^L C_n^2(z)dz\right]^{-3/5}, \qquad l_0 \ll \rho_{\mathrm{pl}} \ll L_0. \tag{113}$$

In the more general Gaussian-beam wave case, the resulting WSF can be approximated by

$$\begin{aligned} D(\rho, L) = 2.91k^2 \Bigg\{ & \rho^{5/3} \int_0^L C_n^2(z) \left|\Theta + \overline{\Theta}\left(\frac{z}{L}\right)\right|^{5/3} dz \\ & + 0.62\Lambda^{11/6}\left(\frac{k}{L}\right)^{1/6} \rho^2 \int_0^L C_n^2(z)\left(1 - \frac{z}{L}\right)^{5/3} dz \Bigg\}, \end{aligned} \tag{114}$$

where we are taking the special case in which $\mathbf{r}_2 = -\mathbf{r}_1$. To deduce the corresponding spatial coherence radius we can use an approximation similar to that employed in obtaining (78), viz., $(k\rho^2/L) \cong (k\rho^2/L)^{5/6}$, which in the present case, leads to

$$\begin{aligned} \rho_0 = \Bigg[\Bigg[& 1.46k^2 \int_0^L C_n^2(z) \Bigg\{ \left|\Theta + \overline{\Theta}\left(\frac{z}{L}\right)\right|^{5/3} \\ & + 0.62\Lambda^{11/6}\left(1 - \frac{z}{L}\right)^{5/3} \Bigg\} dz \Bigg]\Bigg]^{-3/5}, \qquad l_0 \ll \rho_0 \ll L_0. \end{aligned} \tag{115}$$

From (115) we can easily reproduce the plane wave case (113) by setting $\Theta = 1$, $\Lambda = 0$, and obtain the spherical wave case by setting $\Theta = \Lambda = 0$, viz.,

$$\rho_{\mathrm{sp}} = \left[1.46k^2 \int_0^L C_n^2(z)\left(\frac{z}{L}\right)^{5/3} dz\right]^{-3/5}, \qquad l_0 \ll \rho_{\mathrm{sp}} \ll L_0. \tag{116}$$

Here we see the primary difference between the plane wave case (113) and the spherical wave case (116) is that C_n^2 values near the receiver are weighted more heavily for a spherical wave.

6.8.3 Beam wander

Our general expression for beam wander, based on a horizontal path in which C_n^2 can be taken as constant, is given by Eq. (93). The adaptation of this expression to the case of a slant path yields

$$\begin{aligned} \langle r_c^2 \rangle = {} & 7.25L^2 W_0^{-1/3} \int_0^L C_n^2(z)\left(1 - \frac{z}{L}\right)^2 \\ & \times \Bigg[\Bigg[\frac{1}{\left|\Theta_0 + \overline{\Theta}_0\left(1 - \frac{z}{L}\right)\right|^{1/3}} - \left\{ \frac{\kappa_0^2(z) W_0^2}{1 + \kappa_0^2(z) W_0^2 \left[\Theta_0 + \overline{\Theta}_0\left(1 - \frac{z}{L}\right)\right]^2} \right\}^{1/6} \Bigg]\Bigg] dz. \end{aligned} \tag{117}$$

Further simplification of (117) is achieved by considering the case of a collimated beam in which we find that (assuming κ_0, or outer scale, is constant)

$$\langle r_c^2 \rangle = 7.25 L^2 W_0^{-1/3} \left[1 - \left(\frac{\kappa_0^2 W_0^2}{1 + \kappa_0^2 W_0^2} \right)^{1/6} \right] \int_0^L C_n^2(z) \left(1 - \frac{z}{L} \right)^2 dz. \tag{118}$$

6.9 Summary and Discussion

The general characteristics of an optical wave propagating through the atmosphere are greatly affected by small fluctuations in the *refractive index* that are the direct consequence of small temperature fluctuations transported by the turbulent motion of the atmosphere. These atmospheric effects lead to *beam spreading* (both long term and short term), loss of *spatial coherence, angle-of-arrival fluctuations, beam wander, phase fluctuations*, and irradiance fluctuations better known as *scintillation.*

In the general analysis of optical distortions caused by propagating a beam wave through a random medium, it is the first, second, and fourth moments of the optical field that are of greatest concern. Using the *Rytov approximation*, these moments can be calculated with use of the spectral representations derived in Chap. 5 for the first- and second-order complex phase perturbations $\psi_1(\mathbf{r}_1, \mathbf{r}_2)$ and $\psi_2(\mathbf{r}_1, \mathbf{r}_2)$. In particular, it is known that all statistical quantities of interest can be obtained as certain linear combinations of three quantities we denote by $E_1(0,0) = \langle \psi_2(\mathbf{r}, L) \rangle + \frac{1}{2} \langle \psi_1^2(\mathbf{r}, L) \rangle$, $E_2(\mathbf{r}_1, \mathbf{r}_2) = \langle \psi_1(\mathbf{r}_1, L) \psi_1^*(\mathbf{r}_2, L) \rangle$, and $E_3(\mathbf{r}_1, \mathbf{r}_2) = \langle \psi_1(\mathbf{r}_1, L) \psi_1(\mathbf{r}_2, L) \rangle$. These quantities are defined, respectively, for *homogeneous and isotropic turbulence* by the integrals in Eqs. (21)–(23).

In this chapter we have limited our analysis to the first- and second-order field moments for *line-of-sight* propagation in the weak fluctuation regime where the Rytov method is applicable. Most of our results are for a near-ground horizontal path and thus, the structure parameter C_n^2 can be treated as constant. *Weak irradiance fluctuations* are characterized in general by values of the scintillation index (Section 8.2) less than unity, which often limits the propagation path to a few hundred meters or less. In the case of an unbounded plane wave, divergent beam, or collimated beam, it is customary to characterize the weak fluctuation regime by one of the following equivalent conditions:

$$\sigma_R^2 < 1, \quad q < 1, \quad D_{\rm sp}(\sqrt{L/k}) < 1, \tag{119}$$

where $\sigma_R^2 = 1.23 C_n^2 k^{7/6} L^{11/6}$, $q = L/k\rho_{\rm pl}^2$, and $D_{\rm sp}(\rho)$ is the spherical WSF. *Moderate-to-strong fluctuations* arise for propagation distances at which the spatial coherence radius of the optical wave is smaller than the Fresnel scale $\sqrt{L/k}$.

The *first moment* of the field, or *mean field*, is associated with that part of the wave energy that passes through the random medium without distortion. Called the *coherent part* of the field, the mean field takes the form

$$\langle U(\mathbf{r}, L) \rangle = U_0(\mathbf{r}, L) \exp\left(-0.39 C_n^2 k^2 L \kappa_0^{-5/3} \right), \tag{120}$$

where the quantity $U_0(\mathbf{r}, L)$ is the optical field in the absence of turbulence. From this expression it is clear that the mean field is sensitive to the large-scale structure of the random medium and, consequently, approaches zero after short propagation distances. In fact, because all odd moments of the field behave in a similar fashion, it is customary to consider only even moments of the field in most analyses.

The *second moment* (MCF) of the field determines the *spatial coherence* and *mean irradiance* of the field. For the special cases of a plane wave and spherical wave, the MCF leads to

$$\Gamma_2(\mathbf{p}, \mathbf{r}, L) = \begin{cases} \exp\left[-\frac{1}{2}D(\rho, L)\right], & (\text{plane wave}) \\ \frac{1}{(4\pi L)^2}\exp\left[\frac{ik}{L}\mathbf{p}\cdot\mathbf{r} - \frac{1}{2}D(\rho, L)\right], & (\text{spherical wave}) \end{cases} \tag{121}$$

where $D(\rho, L)$ is the WSF for a plane wave or spherical wave defined by (62) or (69). The effects of strong fluctuations on the phase of an unbounded plane or spherical wave are relatively minor, and because the WSF is dominated by phase fluctuations rather than amplitude fluctuations, Eqs. (121) are often used for the MCF for plane waves and spherical waves under all conditions, i.e., even in the presence of saturation.

In general, the MCF for a Gaussian-beam wave is statistically inhomogeneous in that it depends on the positions within the beam profile for the two points, not simply the scalar distance between them. However, in the special case of symmetric points $\mathbf{r}_2 = -\mathbf{r}_1$ the Gaussian-beam wave MCF can be closely approximated by

$$\Gamma_2(\rho, L) = \frac{W_0^2}{W^2}\exp\left[-1.13(q\Lambda)^{5/6} - \frac{1}{4}\Lambda\left(\frac{k\rho^2}{L}\right) - \frac{3}{8}a\left(\frac{qk\rho^2}{L}\right)^{5/6}\right], \quad l_0 \ll \rho \ll L_0, \tag{122}$$

where we assume the separation distance ρ is within the inertial range, a is defined by Eq. (55), and $q = 1.22(\sigma_R^2)^{6/5}$. Unlike the plane wave and spherical wave cases, Eq. (122) is valid only in the weak fluctuation regime. That is, a finite Gaussian-beam wave experiences increased bending of the mean wave front with increases in the level of irradiance fluctuations not accounted for by weak fluctuation theory. This additional bending of the mean wave front, which varies across the beam cross section, causes an increase by diffraction of the spatial coherence radius as compared with that of a spherical wave [35] (see Section 7.3) and also results in longitudinal overfocusing of irradiance in optical receivers [36].

Experimental evidence suggests that, as a Gaussian beam propagates through a random medium, the *mean irradiance* profile remains approximately Gaussian, i.e.,

$$\langle I(\mathbf{r}, L)\rangle \cong \frac{W_0^2}{W_{\mathrm{LT}}^2}\exp[-A_a(\lambda)L - S_a(\lambda)L]\exp\left(-\frac{2r^2}{W_{\mathrm{LT}}^2}\right), \tag{123}$$

where we have also included the attenuation effects of absorption and scattering (recall Section 1.3.2). Here, $A_a(\lambda)$ is an absorption coefficient, $S_a(\lambda)$ is a scattering coefficient, and an estimate of long-term beam spreading or *effective spot size* under weak turbulence conditions is given by (in the absence of inner scale and outer scale effects)

$$W_{\mathrm{LT}} \cong W\sqrt{1+T} = \begin{cases} W\sqrt{1+1.33\sigma_R^2\Lambda^{5/6}}, & C_n^2 = \text{const.} \\ W\sqrt{1+4.35k^{7/6}L^{5/6}\Lambda^{5/6}\int_0^L C_n^2(z)(1-z/L)^{5/3}\,dz}. \end{cases} \tag{124}$$

Under sufficiently weak irradiance fluctuations, the effects of inner scale and outer scale on the beam spot size (124) tend to offset one another. However, this may not always be the case. That is, the presence of a finite outer scale may significantly limit the spreading of the propagating beam, particularly on longer paths. Consequently, for constant values of the structure parameter, it may be preferable to use (47) instead of the upper expression in (124).

Fundamentally, there are two distinct measures of effective spot size called "long term" and "short term." Long-term beam spreading, as described by Eq. (124), is the result of turbulence-induced spreading beyond normal diffraction effects over a long time period and, thus, includes the effects of *beam wander*. The short-term beam spread is roughly the long-term beam spread with the effects of beam wander removed. Hence, the resulting short-term effective spot size can be estimated from the expression (for constant C_n^2)

$$W_{\mathrm{ST}} = W\sqrt{1+1.33\sigma_R^2\Lambda^{5/6} - \langle r_c^2\rangle}, \tag{125}$$

where $\langle r_c^2\rangle$ is the variance of the displacement of the short-term beam spot. *Beam wander* is described in general by the expression

$$\langle r_c^2\rangle = 7.25L^2W_0^{-1/3}\int_0^L C_n^2(z)\left(1-\frac{z}{L}\right)^2 \times \left[\left[\frac{1}{\left|\Theta_0+\overline{\Theta}_0\left(1-\frac{z}{L}\right)\right|^{1/3}} - \left\{\frac{\kappa_0^2(z)W_0^2}{1+\kappa_0^2(z)W_0^2\left[\Theta_0+\overline{\Theta}_0\left(1-\frac{z}{L}\right)\right]^2}\right\}^{1/6}\right]\right] dz, \tag{126}$$

where $\kappa_0(z)$ characterizes the outer scale as a function of propagation distance. For a collimated or focused beam along a horizontal path, this expression reduces to

$$\text{Collimated beam } (\kappa_0 \neq 0): \ \langle r_c^2 \rangle = 2.42 C_n^2 L^3 W_0^{-1/3} \left[1 - \left(\frac{\kappa_0^2 W_0^2}{1 + \kappa_0^2 W_0^2} \right)^{1/6} \right], \tag{127}$$

$$\text{Focused beam } (\kappa_0 \neq 0): \ \langle r_c^2 \rangle = 2.72 C_n^2 L^3 W_0^{-1/3} \left[1 - \frac{8}{9} \left(\frac{\kappa_0^2 W_0^2}{1 + 0.5 \kappa_0^2 W_0^2} \right)^{1/6} \right]. \tag{128}$$

Because large-scale inhomogeneities cause beam wander, the presence of a finite outer scale reduces the available number of large scales, and thus reduces some of the beam wander. This reduction in beam wander variance caused by a finite outer scale is clearly revealed by the analytic forms given in (127) and (128).

The loss of spatial coherence of a beam propagating through turbulence can be determined from the *modulus of the complex degree of coherence*

$$\text{DOC}(\mathbf{r}_1, \mathbf{r}_2, L) = \exp\left[-\frac{1}{2} D(\mathbf{r}_1, \mathbf{r}_2, L) \right], \tag{129}$$

where $D(\mathbf{r}_1, \boldsymbol{r}_2, L)$ is the *wave structure function* (WSF). The WSF for an infinite plane wave and spherical wave can be deduced from Eq. (108) by respectively setting $\Theta = 1$, $\Lambda = 0$ and $\Theta = \Lambda = 0$. Consequently, the implied *spatial coherence radii* obtained from the corresponding WSFs are

$$\text{Plane wave: } \rho_{\text{pl}} = \begin{cases} (1.46 C_n^2 k^2 L)^{-3/5}, & C_n^2 = \text{const.} \\ \left[1.46 k^2 \int_0^L C_n^2(z)\, dz \right]^{-3/5}, & l_0 \ll \rho_{\text{pl}} \ll L_0, \end{cases} \tag{130}$$

$$\text{Spherical wave: } \rho_{\text{sp}} = \begin{cases} (0.55 C_n^2 k^2 L)^{-3/5}, & C_n^2 = \text{const.} \\ \left[1.46 k^2 \int_0^L C_n^2(z)(z/L)^{5/3}\, dz \right]^{-3/5}, & l_0 \ll \rho_{\text{sp}} \ll L_0. \end{cases} \tag{131}$$

For a Gaussian-beam wave, the WSF for constant C_n^2 is given by Eq. (77) and the implied spatial coherence radius is

$$\rho_0 = \begin{cases} \left(\dfrac{3}{1+\Theta+\Theta^2+\Lambda^2}\right)^{1/2} (1.64 C_n^2 k^2 L l_0^{-1/3})^{-1/2}, & \rho_0 \ll l_0, \\ \left[\dfrac{8}{3(a+0.618\Lambda^{11/6})}\right]^{3/5} (1.46 C_n^2 k^2 L)^{-3/5}, & l_0 \ll \rho_0 \ll L_0. \end{cases} \tag{132}$$

Under most conditions, the predicted spatial coherence radius is basically the same for both the von Kármán spectrum and the modified spectrum with high-wave-number bump [19]. In particular, both spectral models predict nearly the same coherence radius when the radius of the first Fresnel zone and initial beam radius are of comparable size and the turbulence is weak. In moderate-to-strong turbulence, however, the modified spectrum predicts a smaller coherence radius (by 8–9%).

Last, the WSF can also be used to calculate the rms *angle of arrival* and corresponding image "dancing" displacement behind a lens of diameter $2W_G$ and focal length f, i.e.,

$$\sqrt{\langle \beta_a^2 \rangle} = \sqrt{2.91 C_n^2 L (2W_G)^{-1/3} [1 - 0.81(2\kappa_0 W_G)^{1/3}]}, \qquad 2W_G \gg l_0, \tag{133}$$

$$\text{rms image displ.} = f\sqrt{2.91 C_n^2 L (2W_G)^{-1/3} [1 - 0.81(2\kappa_0 W_G)^{1/3}]} \qquad 2W_G \gg l_0. \tag{134}$$

6.10 Worked Examples

Example 1: A collimated beam is propagated through atmospheric turbulence to a receiver located 450 meters from the transmitter. Given that $W_0 = 0.5\,\text{cm}$, $\lambda = 0.5\,\mu\text{m}$, and $C_n^2 = 0.5 \times 10^{-13}\,\text{m}^{-2/3}$, assume $l_0 = 0, L_0 = \infty$, and calculate

(*a*) the free-space (no turbulence) spot diameter at the receiver.
(*b*) the spot size diameter of the beam in turbulence at the receiver.
(*c*) the spatial coherence radius ρ_0 at the receiver.
(*d*) What is the corresponding spatial coherence radius for an infinite plane wave and a spherical wave?

Solution: To begin, we first make the calculations:

$$\Lambda_0 = \frac{2L}{kW_0^2} = 2.865, \qquad \Theta = \frac{1}{1+\Lambda_0^2} = 0.1086, \qquad \Lambda = \frac{\Lambda_0}{1+\Lambda_0^2} = 0.311$$

$$a = \frac{\left(1-\Theta^{8/3}\right)}{1-\Theta} = 1.119, \qquad \sigma_R^2 = 1.23 C_n^2 k^{7/6} L^{11/6} = 0.862$$

(*a*) $2W = 2W_0\sqrt{1+\Lambda_0^2} = 3.03\,\text{cm}$
(*b*) $2W_{\text{LT}} = 2W\sqrt{1+1.33\sigma_R^2\Lambda^{5/6}} = 3.63\,\text{cm}$
(*c*) $\rho_0 = \left[0.55C_n^2 k^2 L\left(a+0.62\Lambda^{11/6}\right)\right]^{-3/5} = 0.95\,\text{cm}$
(*d*) $\rho_{\text{pl}} = 0.59\,\text{cm}, \rho_{\text{sp}} = 1.06\,\text{cm}$

❑

Example 2: A collimated beam is propagated through atmospheric turbulence to a receiver located 1 km from the transmitter. Given that the beam radius at the transmitter is 1 cm, the wavelength is 1.55 μm, and the refractive index structure constant is $C_n^2 = 10^{-13}\,\text{m}^{-2/3}$, assume $l_0 = 0, L_0 = \infty$, and use weak fluctuation theory to calculate

(*a*) the spot size W in free space at the receiver,
(*b*) the long-term spot size W_{LT} in turbulence at the receiver,
(*c*) the rms displacement $\sqrt{\langle r_c^2\rangle}$ of the beam hot spot, and
(*d*) the short-term beam radius W_{ST} at the receiver.

Solution: We first calculate the parameters:

$$\Theta_0 = 1 - \frac{L}{F_0} = 1, \qquad \Lambda_0 = \frac{2L}{kW_0^2} = 4.934$$

$$\Theta = \frac{\Theta_0}{\Theta_0^2+\Lambda_0^2} = 0.0395, \qquad \Lambda = \frac{\Lambda_0}{\Theta_0^2+\Lambda_0^2} = 0.1947$$

$$\sigma_R^2 = 1.23C_n^2 k^{7/6} L^{11/6} = 1.99$$

(*a*) $W = \sqrt{\Theta_0^2+\Lambda_0^2} = 5\,\text{cm}$
(*b*) $W_{\text{LT}} = W\sqrt{1+1.33\sigma_R^2\Lambda^{5/4}} = 6.52\,\text{cm}$
(*c*) $\sqrt{\langle r_c^2\rangle} = \sqrt{2.42C_n^2 L^3 W_0^{-1/3}} = 3.35\,\text{cm}$
(*d*) $W_{\text{ST}} = \sqrt{W_{\text{LT}}^2 - \langle r_c^2\rangle} = 5.59\,\text{cm}$

❑

Example 3: Calculate the rms angle-of-arrival and corresponding rms image displacement jitter for an infinite plane wave incident on a telescope aperture of diameter 10 cm and focal length 30 cm. Assume the wavelength is 0.633 μm, the propagation distance is 1 km, and $C_n^2 = 10^{-14}\,\text{m}^{-2/3}$. What is the image displacement jitter if the focal length is 80 cm?

Solution: Directly from the lower expression in (84), we see that the rms angle of arrival is (assuming infinite outer scale)

$$\sqrt{\langle \beta_a^2\rangle} = \sqrt{2.91C_n^2 L(2W_G)^{-1/3}} = 7.92\,\mu\text{rad},$$

and consequently, for a focal length of 30 cm, the rms image displacement jitter is

$$\text{image jitter} = f\sqrt{\langle \beta_a^2\rangle} = 2.38\,\mu\text{m}.$$

If the focal length is 80 cm, we find

$$\text{image jitter} = f\sqrt{\langle \beta_a^2 \rangle} = 6.33\,\mu\text{m}.$$

❑

Example 4: Compare the rms beam wander displacement for a collimated beam and a convergent beam, both with wavelength 1.55 μm and beam diameter 10 cm at the transmitter. Assume the receiver is located 1 km from the transmitter, the convergent beam is focused at 900 m, and $C_n^2 = 5 \times 10^{-14}\,\text{m}^{-2/3}$. Neglect the effects of inner scale and outer scale.

Solution: For the collimated beam we can use Eq. (95) for our calculation, from which we find

$$\sqrt{\langle r_c^2 \rangle} = \sqrt{2.42 C_n^2 L^3 W_0^{-1/3}}$$
$$= 1.81\,\text{cm}.$$

However, we must use Eq. (94) for computing beam wander displacement of the convergent beam (which is not focused at the receiver). Consequently, for the convergent beam case, the corresponding expression is

$$\sqrt{\langle r_c^2 \rangle} = \sqrt{2.42 C_n^2 L^3 W_0^{-1/3} \text{Re}\left[{}_2F_1\left(\frac{1}{3}, 1; 4;\ 1 - |\Theta_0|\right)\right]}$$
$$= 1.90\,\text{cm}.$$

As expected, the rms beam wander displacement for the convergent beam is somewhat larger than that of the collimated beam. Although these rms displacements are similar for the two beams, the implied effect on the scintillation index (Chap. 8) will be found to be quite different. That is, because the long-term spot radius in the case of the collimated beam is $W_{\text{LT}} = 5.88\,\text{cm}$, the rms beam wander displacement is roughly 31% of the beam spot size radius. In the case of the convergent beam, however, we find $W_{\text{LT}} = 2.55\,\text{cm}$, and here the rms beam wander displacement is approximately 75% of the beam spot size radius—a significant difference.

❑

Example 5: (NUMERICAL) Graphically compare the mean irradiance profiles predicted by

(*a*) the exact expression (40): $\langle I(\mathbf{r}, L) \rangle = \dfrac{W_0^2}{W^2} \exp\left(-\dfrac{2r^2}{W^2}\right) \exp\left[2\sigma_r^2(\mathbf{r}, L) - T\right]$

and

(*b*) the Gaussian approximation (45): $\langle I(\mathbf{r}, L) \rangle = \dfrac{W_0^2}{W_{\text{LT}}^2} \exp\left(-\dfrac{2r^2}{W_{\text{LT}}^2}\right)$.

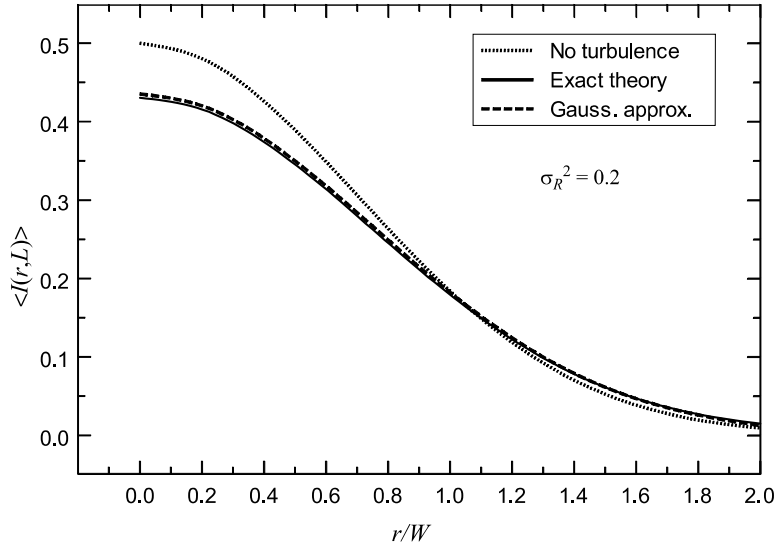

Figure 6.9 Mean irradiance profile of a collimated beam ($\Theta_0 = \Lambda_0 = 1$) as predicted by Eqs. (40) and (45) and that in the absence of turbulence.

Solution: Let us assume the Rytov variance is $\sigma_R^2 = 0.2$, consistent with weak fluctuation theory. In Fig. 6.9 we show the results of Eq. (40) (solid curve), Eq. (45) (dashed curve), and the diffractive irradiance profile that would exist in the absence of turbulence (dotted curve). From the graph, we see that atmospheric turbulence causes a decrease in the on-axis irradiance, but also that the Gaussian profile (45) is a good approximation to the mean irradiance described by (40) under weak fluctuation conditions.

❑

Example 6: (NUMERICAL) For symmetric points $\mathbf{r}_2 = -\mathbf{r}_1$, the normalized MCF of a Gaussian-beam wave can be written as

$$\frac{\Gamma_2(\rho, L)}{\Gamma_2(0, L)} = \exp\left[\left[-\frac{1}{4}\Lambda R^2 - 3(q\Lambda)^{5/6}\int_0^1 \xi^{5/3}\left\{{}_1F_1\left[-\frac{5}{6}; 1; -\frac{(1-\overline{\Theta}\xi)^2 R^2}{4\Lambda\xi^2}\right] - 1\right\} d\xi\right]\right],$$

where $R = (k\rho^2/L)^{1/2}$ and ${}_1F_1$ denotes a confluent hypergeometric function. For collimated beam waves characterized by $\Theta_0 = 1$, $\Lambda_0 = 1$; $\Theta_0 = 1$, $\Lambda_0 = 10$; and $\Theta_0 = 0.1$, $\Lambda_0 = 1$ and atmospheric conditions characterized by $q = 0.1$, write a software program to calculate the above expression for $R = 1$, 2, 3, and 4. Compare these results with the approximation given by Eq. (54).

Solution: Any software program that contains the confluent hypergeometric function as a built-in function is suitable for this calculation. The required computations then lead to the numerical values provided in the tables below:

Table 6.2 $\Theta_0 = 1,\ \Lambda_0 = 1$

	$R = 1$	$R = 2$	$R = 3$	$R = 4$
Exact:	0.8176	0.4645	0.1883	0.0552
Approximation:	0.8043	0.4518	0.1820	0.0531

Table 6.3 $\Theta_0 = 1,\ \Lambda_0 = 10$

	$R = 1$	$R = 2$	$R = 3$	$R = 4$
Exact:	0.9265	0.7636	0.5694	0.3868
Approximation:	0.9228	0.7592	0.5657	0.3843

Table 6.4 $\Theta_0 = 0.1,\ \Lambda_0 = 1$

	$R = 1$	$R = 2$	$R = 3$	$R = 4$
Exact:	0.7434	0.3133	0.0760	0.0107
Approximation:	0.7346	0.3062	0.0737	0.0103

Problems

Section 6.2

1. The confluent hypergeometric function of the second kind has the integral representation

$$U(a;c;x) = \frac{1}{\Gamma(a)}\int_0^\infty e^{-xt}t^{a-1}(1+t)^{c-a-1}dt, \qquad a>0, x>0.$$

Use this result to show that

$$\int_0^\infty \kappa^{2\mu}\frac{\exp\left(-\kappa^2/\kappa_m^2\right)}{(\kappa_0^2+\kappa^2)^{11/6}}\,d\kappa = \frac{1}{2}\kappa_0^{2\mu-8/3}\Gamma\left(\mu+\frac{1}{2}\right)U\left(\mu+\frac{1}{2};\ \mu-\frac{1}{3};\frac{\kappa_0^2}{\kappa_m^2}\right).$$

2. Use the von Kármán spectrum (28) and the result of Prob. 1 to deduce that

(*a*) $E_1(0,0) = -0.033\pi^2 C_n^2 k^2 L\kappa_0^{-5/3}U\left(1;\frac{1}{6};\frac{\kappa_0^2}{\kappa_m^2}\right)$.

(*b*) Use the asymptotic relation (30) to obtain the result

$$E_1(0,0) \cong -0.39C_n^2 k^2 L\kappa_0^{-5/3}, \qquad \kappa_0^2/\kappa_m^2 \ll 1.$$

3. Show that Eqs. (66) and (67) in Chap. 5 reduce to Eqs. (25) and (26) in the present chapter.

4. By use of the identity

$$\langle\exp(\psi)\rangle = \exp\left[\langle\psi\rangle + \frac{1}{2}(\langle\psi^2\rangle - \langle\psi\rangle^2)\right],$$

deduce the following results, retaining only terms of second order or less:

(*a*) $\langle\exp[\psi(\mathbf{r},L)]\rangle = \exp[E_1(0,0)]$.

(*b*) $\langle\exp[\psi(\mathbf{r}_1,L)+\psi^*(\mathbf{r}_2,L)]\rangle = \exp[2E_1(0,0)+E_2(\mathbf{r}_1,\mathbf{r}_2)]$.

(*c*) $\langle\exp[\psi(\mathbf{r}_1,L)+\psi^*(\mathbf{r}_2,L)+\psi(\mathbf{r}_3,L)+\psi^*(\mathbf{r}_4,L)]\rangle$

$$= \exp\Big[4E_1(0,0)+E_2(\mathbf{r}_1,\mathbf{r}_2)+E_2(\mathbf{r}_1,\mathbf{r}_4)+E_2(\mathbf{r}_3,\mathbf{r}_2) + E_2(\mathbf{r}_3,\mathbf{r}_4)+E_3(\mathbf{r}_1,\mathbf{r}_3)+E_3^*(\mathbf{r}_2,\mathbf{r}_4)\Big].$$

5. Show that, in the limiting case of a plane wave, Eqs. (25) and (26) reduce to

$$E_2(\mathbf{r}_1,\mathbf{r}_2) = 4\pi^2 k^2 L\int_0^\infty \kappa\Phi_n(\kappa)\,J_0(\kappa\rho)\,d\kappa,$$

$$E_3(\mathbf{r}_1,\mathbf{r}_2) = -4\pi^2 k^2 L\int_0^1\int_0^\infty \kappa\Phi_n(\kappa)J_0(\kappa\rho)\exp\left(-\frac{i\kappa^2 L\xi}{k}\right)d\kappa\,d\xi.$$

6. Show that, in the limiting case of a spherical wave, Eqs. (25) and (26) reduce to

$$E_2(\mathbf{r}_1,\mathbf{r}_2) = 4\pi^2 k^2 L \int_0^1 \int_0^\infty \kappa \Phi_n(\kappa) J_0(\kappa\xi\rho)\, d\kappa\, d\xi,$$

$$E_3(\mathbf{r}_1,\mathbf{r}_2) = -4\pi^2 k^2 L \int_0^1 \int_0^\infty \kappa \Phi_n(\kappa) J_0(\kappa\xi\rho) \exp\left[-\frac{i\kappa^2 L}{k}\xi(1-\xi)\right] d\kappa\, d\xi.$$

7. Use the modified atmospheric spectrum [Eq. (22) in Chap. 3] and the technique illustrated in Section 6.2.3 to derive the mean field $\langle U(\mathbf{r}, L)\rangle$.

Section 6.3

8. Verify that the free-space MCF satisfies

$$\Gamma_2^0(\mathbf{r}_1,\mathbf{r}_2,L) = U_0(\mathbf{r}_1,L)U_0^*(\mathbf{r}_2,L) = \frac{W_0^2}{W^2}\exp\left(-\frac{2r^2}{W^2} - \frac{\rho^2}{2W^2} - i\frac{k}{F}\mathbf{p}\cdot\mathbf{r}\right).$$

9. Use the Kolmogorov spectrum (41) and the Maclaurin series representation

$$I_0(2\Lambda r\kappa\xi) - 1 = \sum_{n=1}^{\infty} \frac{(\Lambda r)^{2n}}{(n!)^2}\kappa^{2n}\xi^{2n}$$

(*a*) to show that Eq. (37) takes the form (assume termwise integration is permitted)

$$\sigma_r^2(\mathbf{r},L) = 0.651 C_n^2 k^2 L \sum_{n=1}^{\infty} \frac{(\Lambda r)^{2n}}{(n!)^2} \int_0^1 \xi^{2n} \int_0^\infty \kappa^{2n-8/3} \exp\left(-\frac{\Lambda L\kappa^2\xi^2}{k}\right) d\kappa\, d\xi.$$

(*b*) Use properties of the gamma function (see Appendix I) to deduce that

$$\int_0^\infty \kappa^{2n-8/3} \exp(-a^2\kappa^2)\, d\kappa = \frac{1}{2}\Gamma(n-5/6)a^{5/3-2n}.$$

(*c*) Finally, use the result of part (*b*) to show that the expression in (*a*) can be reduced to

$$\sigma_r^2(\mathbf{r},L) = 0.122\Gamma(-5/6)C_n^2 k^{7/6} L^{11/6}\Lambda^{5/6}\left[\sum_{n=0}^{\infty}\frac{(-5/6)_n}{(1)_n n!}\left(\frac{2r^2}{W^2}\right)^n - 1\right]$$

$$= 0.816 C_n^2 k^{7/6} L^{11/6}\Lambda^{5/6}\left[1 - {}_1F_1\left(-\frac{5}{6}; 1; \frac{2r^2}{W^2}\right)\right],$$

where $(a)_n = \Gamma(a+n)/\Gamma(a)$ is the Pochhammer symbol (see Appendix I).

10. Use the von Kármán spectrum and the result of Probs. 1 and 2 to deduce the value of the integral

$$E_2(0,0) = 4\pi^2 k^2 L \int_0^1 \int_0^\infty \kappa \Phi_n(\kappa) e^{-\Lambda L \kappa^2 \xi^2 / k}\, d\kappa\, d\xi$$

and, consequently, to show that in the limit $\kappa_0^2/\kappa_m^2 \to 0$ (assume the inner scale vanishes while at the same time the outer scale becomes infinite) that

$$T = -2E_1(0,0) - E_2(0,0) \cong 1.33\sigma_R^2 \Lambda^{5/6}.$$

11. Expand the Bessel function in Eq. (53) in a Maclaurin series and use the Kolmogorov spectrum to deduce that

$$d(\rho, L) = 6(q\Lambda)^{5/6} \int_0^1 \xi^{5/3} \left\{ {}_1F_1\left[-\frac{5}{6};\ 1;\ -\frac{(1-\overline{\Theta}\xi)^2 R^2}{4\Lambda\xi^2} \right] - 1 \right\} d\xi,$$

where $R^2 = k\rho^2/L$ and $q = 1.22(\sigma_R^2)^{6/5}$.

12. A collimated beam is propagated through atmospheric turbulence to a receiver 1 km from the transmitter. If $W_0 = 1\,\text{cm}, \lambda = 0.63\,\mu\text{m}$, and $C_n^2 = 5 \times 10^{-14}\,\text{m}^{-2/3}$,
(*a*) calculate the diffractive spot radius W at the receiver.
(*b*) calculate the effective or long-term spot radius W_{LT} at the receiver.

13. Repeat Prob. 12 for a focused beam.

Section 6.4

14. Calculate the spatial coherence radius for the beam and conditions given in Prob. 12. What is the corresponding spatial coherence radius for an infinite plane wave and a spherical wave? Use the Kolmogorov spectrum (41).

15. The number of "speckle cells" on a receiver aperture of diameter $2W_G$ can be approximated by comparing the ratio of areas of the receiver lens and spatial coherence cell, i.e.,

$$N_S = 1 + \frac{A_{\text{lens}}}{A_{\text{coh rad}}} = 1 + \left(\frac{W_G}{\rho_0} \right)^2.$$

To ensure 100 speckle cells on the receiver aperture, what size aperture is required for a collimated beam with radius $W_0 = 0.5\,\text{cm}$, wavelength $\lambda = 0.5\,\mu\text{m}$, propagation distance $L = 800\,\text{m}$, and structure constant $C_n^2 = 7.5 \times 10^{-14}\,\text{m}^{-2/3}$?

16. Expand the Bessel function in Eq. (58) in a Maclaurin series and, using the von Kármán spectrum (28),

(*a*) show that the plane wave structure function can be written as

$$D_{\rm pl}(\rho,L)=1.30C_n^2k^2L\kappa_0^{-5/3}\sum_{n=1}^{\infty}\frac{(-1)^{n-1}}{n!}(\kappa_0\rho/2)^{2n}U\left(n+1;n+\frac{1}{6};\frac{\kappa_0^2}{\kappa_m^2}\right).$$

Hint: See Prob. 1

(*b*) For $\kappa_0 \to 0$, use Eq. (30) to show that the first term of the series in part (*a*) reduces the expression to

$$D_{\rm pl}(\rho,L)\cong 3.28C_n^2k^2Ll_0^{-1/3}\rho^2,\qquad \rho\ll l_0.$$

(*c*) For $\kappa_0 \neq 0$, show that the series in (*a*) sums to

$$D_{\rm pl}(\rho,L)=1.303C_n^2k^2L\times\left\{\Gamma(-5/6)\kappa_m^{-5/3}\left[1-{}_1F_1\left(-\frac{5}{6};1;-\frac{\kappa_m^2\rho^2}{4}\right)\right]-\frac{9}{5}\kappa_0^{1/3}\rho^2\right\}.$$

17. Use asymptotic formulas of the confluent hypergeometric function in the general expression given in part (*c*) of Prob. 16 to deduce the results

$$D_{\rm pl}(\rho,L)=\begin{cases}3.28C_n^2k^2Ll_0^{-1/3}\rho^2\left[1-0.72(\kappa_0 l_0)^{1/3}\right], & \rho\ll l_0,\\ 2.91C_n^2k^2L\rho^{5/3}\left[1-0.81(\kappa_0\rho)^{1/3}\right], & \rho\gg l_0.\end{cases}$$

18. Verify that the modulus of the complex degree of coherence (56) reduces to

$$\mathrm{DOC}(\mathbf{r}_1,\mathbf{r}_2,L)=\exp\left[-\frac{1}{2}D(\mathbf{r}_1,\mathbf{r}_2,L)\right],$$

where $D(\mathbf{r}_1, \mathbf{r}_2, L)$ is the WSF of a Gaussian-beam wave.

19. Follow the approach in Prob. 16 to reduce the WSF for a spherical wave (67) to

$$D_{\rm sp}(\rho,L)=1.303C_n^2k^2L\left\{\Gamma(-5/6)\kappa_m^{-5/3}\times\left[1-{}_2F_2\left(-\frac{5}{6},\frac{1}{2};1,\frac{3}{2};-\frac{\kappa_m^2\rho^2}{4}\right)\right]-\frac{3}{5}\kappa_0^{1/3}\rho^2\right\}.$$

20. Given that the inner scale and outer scale are, respectively, 5 mm and 1 m, what is the spatial coherence radius of a plane wave ($\lambda = 1\ \mu$m) at the receiver

(*a*) based on a von Kármán spectrum, propagation path length $L = 750$ m, and structure constant $C_n^2 = 10^{-13}\ \mathrm{m}^{-2/3}$?

(*b*) What is the spatial coherence radius for a spherical wave over the same propagation path?

Ans. (*a*) $\rho_{\rm pl} = 6.58$ mm (*b*) $\rho_{\rm sp} = 11.8$ mm

21. Use the relation $\chi(\mathbf{r},L)=\frac{1}{2}[\psi(\mathbf{r},L)+\psi^*(\mathbf{r},L)]$

(*a*) to deduce that

$$\langle \chi(\mathbf{r}_1, L)\chi(\mathbf{r}_2, L)\rangle = \frac{1}{2}\mathrm{Re}[E_2(\mathbf{r}_1, \mathbf{r}_2) + E_3(\mathbf{r}_1, \mathbf{r}_2)].$$

(*b*) For the special case of a plane wave (Prob. 5), show that

$$\langle \chi(\mathbf{r}_1, L)\chi(\mathbf{r}_2, L)\rangle = 2\pi^2 k^2 L \int_0^1 \int_0^\infty \kappa \Phi_n(\kappa) J_0(\kappa\rho)\left[1 - \cos\left(\frac{L\kappa^2\xi}{k}\right)\right] d\kappa\, d\xi.$$

22. The log-amplitude structure function is defined by the ensemble average

$$D_\chi(\mathbf{r}_1, \mathbf{r}_2, L) = \langle [\chi(\mathbf{r}_1, L) - \chi(\mathbf{r}_2, L)]^2\rangle.$$

For the limiting case of a plane wave, show that

$$\begin{aligned} D_\chi(\mathbf{r}_1, \mathbf{r}_2, L) &\equiv D_\chi(\rho, L) \\ &= 4\pi^2 k^2 L \int_0^1 \int_0^\infty \kappa \Phi_n(\kappa)[1 - J_0(\kappa\rho)]\left[1 - \cos\left(\frac{L\kappa^2\xi}{k}\right)\right] d\kappa\, d\xi. \end{aligned}$$

Hint: Use the results of Prob. 21.

23. Use the relation $S(\mathbf{r}, L) = \frac{1}{2i}[\psi(\mathbf{r}, L) - \psi^*(\mathbf{r}, L)]$
(*a*) to deduce that

$$\langle S(\mathbf{r}_1, L)S(\mathbf{r}_2, L)\rangle = \frac{1}{2}\mathrm{Re}[E_2(\mathbf{r}_1, \mathbf{r}_2) - E_3(\mathbf{r}_1, \mathbf{r}_2)].$$

(*b*) For the special case of a plane wave, use Prob. 5 to show that

$$\langle S(\mathbf{r}_1, L)S(\mathbf{r}_2, L)\rangle = 2\pi^2 k^2 L \int_0^1 \int_0^\infty \kappa \Phi_n(\kappa) J_0(\kappa\rho)\left[1 + \cos\left(\frac{L\kappa^2\xi}{k}\right)\right] d\kappa\, d\xi.$$

24. The phase structure function is defined by the ensemble average

$$D_S(\mathbf{r}_1, \mathbf{r}_2, L) = \langle [S(\mathbf{r}_1, L) - S(\mathbf{r}_2, L)]^2\rangle.$$

For the limiting case of a plane wave, show that

$$\begin{aligned} D_S(\mathbf{r}_1, \mathbf{r}_2, L) &\equiv D_S(\rho, L) \\ &= 4\pi^2 k^2 L \int_0^1 \int_0^\infty \kappa \Phi_n(\kappa)[1 - J_0(\kappa\rho)]\left[1 + \cos\left(\frac{L\kappa^2\xi}{k}\right)\right] d\kappa\, d\xi. \end{aligned}$$

Hint: Use the results of Prob. 23.

25. For the limiting case of a spherical wave, show that the phase structure function is given by

$$D_S(\mathbf{r}_1,\mathbf{r}_2,L)\equiv D_S(\rho,L)$$
$$=4\pi^2k^2L\int_0^1\int_0^\infty \kappa\Phi_n(\kappa)[1-J_0(\kappa\xi\rho)]\left\{1+\cos\left[\frac{L\kappa^2}{k}\xi(1-\xi)\right]\right\}d\kappa d\xi.$$

26. Based on the integral representation given in Prob. 24, use the Tatarskii spectrum to deduce the asymptotic behavior of the phase structure function for a plane wave given by

$$D_S(\rho,L)=\begin{cases}1.64C_n^2k^2Ll_0^{-1/3}\left[1+0.64(kl_0^2/L)^{1/6}\right]\rho^2, & \rho\ll l_0,\\ 1.46C_n^2k^2L\rho^{5/3}, & l_0\ll\rho\ll(L/k)^{1/2},\\ 2.91C_n^2k^2L\rho^{5/3}, & (L/k)^{1/2}\ll\rho\ll L_0.\end{cases}$$

27. From Eq. (78) with $q=1.22(\sigma_R^2)^{6/5}$, deduce that

$$\frac{\rho_0}{2W}=0.35\left(\frac{\Lambda}{q}\right)^{1/2}\left[\frac{8}{3(a+0.62\Lambda^{11/6})}\right]^{3/5},\qquad l_0\ll\rho_0\ll L_0.$$

Section 6.5

28. For a Gaussian-beam wave, show that the variance of the angle-of-arrival fluctuations over an aperture of radius W_G leads to

$$\langle\beta_a^2\rangle\cong 1.09C_n^2L(2W_G)^{-1/3}\left[a+0.62\Lambda^{11/6}\left(\frac{4kW_G^2}{L}\right)^{1/3}\right],$$
$$\sqrt{L/k}\ll 2W_G.$$

29. Given the result of Prob. 28 for a Gaussian-beam wave, deduce the corresponding expression for a spherical wave.

30. A large collimated beam is propagated through atmospheric turbulence to a receiver 1 km from the transmitter. If $\lambda=1.55\ \mu$m and $C_n^2=7.5\times10^{-14}$, calculate
    (*a*) the rms angle-of-arrival given that the receiver aperture is $2W_G=5$ cm.
    (*b*) the rms image jitter (displacement) given that the receiver aperture has a focal length of 10 cm.
    (*c*) Find the rms angle of arrival and rms image jitter given that the receiver aperture is increased to 10 cm and the focal length is 50 cm.

Section 6.6

31. For a collimated beam propagating 1.5 km through atmospheric turbulence with $W_0=1$ cm, $\lambda=1.55\ \mu$m, $\kappa_0=0$, and $C_n^2=7.5\times10^{-14}$, calculate
    (*a*) the rms displacement of the short-term beam centroid at the receiver.

(*b*) the short-term beam radius at the receiver.
(*c*) What is the rms angular beam wander in microradians?

Hint: In part (*c*), use the small angle approximation $\tan\theta \cong \theta, \theta \ll 1$.

32. Repeat Prob. 31 when the outer scale parameter
(*a*) $\kappa_0 = 1$.
(*b*) $\kappa_0 = 2$.

33. Calculate the rms displacement of a beam focused at the receiver that has propagated 1 km. Assume $W_0 = 5\,\text{cm}, \lambda = 1.55\,\mu\text{m}, C_n^2 = 7.5 \times 10^{-14}$, and
(*a*) $\kappa_0 = 0$.
(*b*) $\kappa_0 = 2$.

34. For the beam described in Prob. 33, use $\kappa_0 = 6$ and calculate the long-term and short-term beam radii.

35. Given the long-term association $\sigma_r^2(\mathbf{r}, L) \cong Tr^2/W^2$, use beam wander relations to deduce that the short-term association is $\sigma_r^2(\mathbf{r}, L)_{\text{ST}} \cong (T - \langle r_c^2\rangle/W^2)(r^2/W^2)$.

36. Given a collimated beam and the filter function defined by (91),
(*a*) show that, by retaining diffraction effects, the displacement variance for beam wander becomes ($\kappa_0 = 0$)

$$\langle r_c^2\rangle = 1.303\Gamma(1/6)C_n^2L^3W_0^{-1/3}\int_0^1 \xi^2\left[1 + \Lambda_0^2(1-\xi)^2\right]^{-1/6} d\xi.$$

(*b*) Perform the integration in part (*a*) and show that it leads to

$$\int_0^1 \xi^2\left[1 + \Lambda_0^2(1-\xi)^2\right]^{-1/6} d\xi = \frac{6}{5\Lambda_0^2} - \frac{33(1+\Lambda_0^2)^{5/6}}{40\Lambda_0^2} + \frac{5(8\Lambda_0^2 - 3)}{40\Lambda_0^2}\,{}_2F_1\left(\frac{1}{2}, \frac{1}{6}; \frac{3}{2}; -\Lambda_0^2\right).$$

(*c*) From the result in part (*b*), show that the displacement variance becomes

$$\langle r_c^2\rangle = 0.18C_n^2L^3W_0^{-1/3}\Lambda_0^{-2}\left[48 - 33(1+\Lambda_0^2)^{5/6} + 5(8\Lambda_0^2 - 3)\,{}_2F_1\left(\frac{1}{2}, \frac{1}{6}; \frac{3}{2}; -\Lambda_0^2\right)\right].$$

37. Use the result given in part (*c*) of Prob. 36 to
(*a*) determine the displacement variance for the beam wave described in Prob. 31
(*b*) Compare the answer in Part (*a*) with the result of Eq. (95).

38. What does the expression in part (*c*) of Prob. 36 reduce to in the limiting case of a spherical wave ($\Lambda_0 \to \infty$)?

Section 6.7

39. Use the Kolmogorov spectrum to verify the result of Eq. (102).

40. Use the Kolmogorov spectrum to verify the result of Eq. (103).

41. Consider a slant path from the ground to the top of a building 500 m high and at zenith angle 80 degrees from the observer. Assume $C_n^2(h) = A\exp(-h/100)$, where $A = 1.7 \times 10^{-13}\,\mathrm{m}^{-2/3}$ and h is the altitude from ground level. Given an uplink collimated laser beam with spot radius $W_0 = 1$ cm and wavelength $\lambda = 1.55\ \mu$m, ignore the effects of inner scale and outer scale, and
    (*a*) calculate the free-space and long-term beam radius at the top of the building.
    (*b*) Calculate the spatial coherence radius of the beam at the top of the building.

    Ans. (*a*) $W = 14.2\,\mathrm{cm}, W_{\mathrm{LT}} = 15.8\,\mathrm{cm}$ (*b*) $\rho_0 = 10.9\,\mathrm{cm}$

42. Given the slant path scenario described in Prob. 41, consider now the case where the transmitter is on top of the building and the receiver is on the ground.
    (*a*) Calculate the free-space and long-term beam radius at the receiver.
    (*b*) Calculate the spatial coherence radius of the beam at the receiver.

43. Given the slant path scenario described in Prob. 41, use Eq. (112) to calculate the beam wander displacement for the uplink path in the case of an infinite outer scale.

44. Repeat Prob. 43 for the case of a focused beam using Eq. (111).

45. Solve Probs. 42 and 43 for the case when the beam radius is increased to 2 cm and the wavelength is 1.06 μm.

References

1. L. A. Chernov, *Wave Propagation in a Random Medium* (McGraw-Hill, New York,1960), trans. by R. A. Silverman.
2. V. I. Tatarskii, *Wave Propagation in a Turbulent Medium* (McGraw-Hill, New York, 1961), trans. by R. A. Silverman.
3. R. S. Lawrence and J. W. Strohbehn, "A survey of clear-air propagation effects relevant to optical communications," *Proc. IEEE* **58**, 1523–1545 (1970).
4. R. F. Lutomirski and H. T. Yura, "Propagation of a finite optical beam in an inhomogeneous medium," *Appl. Opt.* **10**, 1652–1658 (1971).
5. A. M. Prokhorov, F. V. Bunkin, K. S. Gochelashvily, and V. I. Shishov, "Laser irradiance in turbulent media," *Proc. IEEE* **63**, 790–809 (1975).
6. R. L. Fante, "Electromagnetic beam propagation in turbulent media," *Proc. IEEE* **63**, 1669–1692 (1975).
7. A. Ishimaru, *Wave Propagation and Scattering in Random Media* (IEEE Press, Piscataway, NJ, 1997); [previously published as Vols I & II by Academic, New York (1978)].
8. R. Dashen, "Path integrals for waves in random media," *J. Math. Phys.* **20**, 894–920 (1979).
9. V. I. Tatarskii and V. U. Zavorotnyi, "Strong fluctuations in light propagation in a randomly inhomogeneous medium," in *Progress in Optics III*, E. Wolf, ed. (Elsevier, New York, 1980).
10. R. L. Fante, "Electromagnetic beam propagation in turbulent media: an update," *Proc. IEEE* **68**, 1424–1443 (1980).
11. R. L. Fante, "Wave propagation in random media: a systems approach," in *Progress in Optics XXII*, E. Wolf, ed. (Elsevier, New York, 1985).
12. H. T. Yura, C. C. Sung, S. F. Clifford, and R. J. Hill, "Second-order Rytov approximation," *J. Opt. Soc. Am.* **73**, 500–502 (1983).
13. H. T. Yura and S. G. Hanson, "Second-order statistics for wave propagation through complex optical systems," *J. Opt. Soc. Am. A* **6**, 564–575 (1989).
14. A. Stuart and J. K. Ord, *Kendall's Advanced Theory of Statistics*, 5th ed., Vol. 1 (Oxford University Press, New York, 1987).
15. L. C. Andrews, *Special Functions of Mathematics for Engineers*, 2nd ed. (SPIE Optical Engineering Press, Bellingham, Wash.; Oxford University Press, Oxford, 1998); [formerly published as 2nd ed. by McGraw-Hill, New York (1992)].
16. L. C. Andrews and W. B. Miller, "Single-pass and double-pass propagation through complex paraxial optical systems," *J. Opt. Soc. Am. A* **12**, 137–150 (1995); "Single-pass and double-pass propagation through complex paraxial optical systems: Errata," *J. Opt. Soc. Am. A* **12**, 2213 (1995).
17. L. C. Andrews, W. B. Miller, and J. C. Ricklin, "Spatial coherence of a Gaussian-beam wave in weak and strong optical turbulence," *J. Opt. Soc. Am. A* **11**, 1653–1660 (1994).

18. W. B. Miller, J. C. Ricklin, and L. C. Andrews, "Log-amplitude variance and wave structure function: a new perspective for Gaussian beams," *J. Opt. Soc. Am. A* **10**, 661–672 (1993).
19. C. Y. Young and L. C. Andrews, "Effects of a modified spectral model on the spatial coherence of a laser beam," *Waves in Random Media* **4**, 385–397 (1994).
20. L. C. Andrews, S. Vester, and C. E. Richardson, "Analytic expressions for the wave structure function based on a bump spectral model for refractive index fluctuations," *J. Mod. Opt.* **40**, 931–938 (1993).
21. J. H. Churnside and R. J. Lataitis, "Wander of an optical beam in the turbulent atmosphere," *Appl. Opt.* **29**, 926–930 (1990).
22. L. A. Chernov, *Wave Propagation in a Random Medium* (Dover, New York, 1967).
23. P. Beckmann, "Signal degeneration in laser beams propagated through a turbulent atmosphere," *Radio Sci.* **69**D, 629–640 (1965).
24. R. Esposito, "Power scintillations due to the wandering of the laser beam," *Proc. IEEE* **55**, 1533–1534 (1967).
25. T. Chiba, "Spot dancing of the laser beam propagated through the turbulent atmosphere," *Appl. Opt.* **10**, 2456–2461 (1971).
26. V. I. Klyatskin and A. I. Kon, "On the displacement of spatially bounded light beams in a turbulent medium in the Markovian-random-process approximation," *Radiofiz. Quantum Electron.* **15**, 1056–1061 (1972).
27. J. R. Kerr and J. R. Dunphy, "Experimental effects of finite transmitter apertures on scintillations," *J. Opt. Soc. Am.* **63**, 1–8 (1973).
28. D. L. Fried, "Statistics of laser beam fade induced by pointing jitter," *Appl. Opt.* **12**, 422–423 (1973).
29. P. J. Titterton, "Power reduction and fluctuations caused by narrow laser beam motion in the far field," *Appl. Opt.* **12**, 423–425 (1973).
30. V. L. Mironov and V. V. Nosov, "On the theory of spatially limited light beam displacements in a randomly inhomogeneous medium," *J. Opt. Soc. Am.* **67**, 1073–1080 (1977).
31. L. C. Andrews, R. L. Phillips, R. J. Sasiela, and R. Parenti, "Beam wander effects on the scintillation index of a focused beam," Proc. SPIE **5793** (2005).
32. M. T. Tavis and H. T. Yura, "Short-term average irradiance profile of an optical beam in a turbulent medium," *Appl. Opt.* **15**, 2922–2931 (1976).
33. D. H. Tofsted, "Outer-scale effects on beam-wander and angle-of-arrival variances," *Appl. Opt.* **31**, 5865–5870 (1992).
34. J. W. Goodman, *Introduction to Fourier Optics* (McGraw-Hill, New York, 1968).
35. M. S. Belen'kii, A. I. Kon, and V. L. Mironov, "Turbulent distortions of the spatial coherence of a laser beam," *Sov. J. Quantum Electron.* **7**, 287–290 (1977).
36. M. S. Belen'kii, V. L. Mironov, V. I. Sazanovich, and R. Sh. Tswyk, "Longitudinal overfocusing of radiation in optical receivers," *Opt. Lett.* **10**, 255–257 (1985).